Article

Cell Chemical Biology

# The Antimalarial Natural Product Salinipostin A Identifies Essential α/β Serine Hydrolases Involved in Lipid Metabolism in *P. falciparum* Parasites

## Graphical Abstract

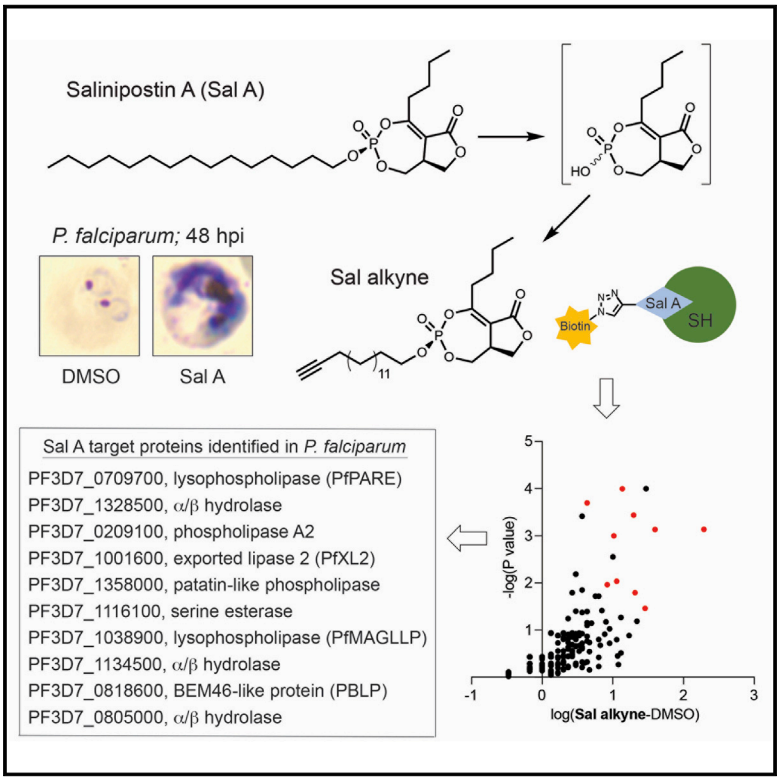


## Highlights

- Semi-synthesis of an affinity analog of the antimalarial natural product Sal A
- Identification of serine hydrolases as the primary targets of Sal A in *P. falciparum*
- Sal A covalently binds to and inhibits a MAGL-like protein in *P. falciparum*
- Parasites are unable to generate strong *in vitro* resistance to Sal A

## Authors

Euna Yoo, Christopher J. Schulze, Barbara H. Stokes, ..., Eranthie Weerapana, David A. Fidock, Matthew Bogyo

## Correspondence

mbogyo@stanford.edu

## In Brief

Using a probe analog of the antimalarial natural product Sal A, Yoo et al. identify its targets as multiple essential serine hydrolases, including a homolog of human monoacylglycerol lipase. Because parasites were unable to generate robust *in vitro* resistance to Sal A, these enzymes represent promising targets for antimalarial drugs.

Yoo et al., 2020, Cell Chemical Biology *27*, 143–157
February 20, 2020 
https://doi.org/10.1016/j.chembiol.2020.01.001

CellPress

Cell Chemical Biology
Article

# The Antimalarial Natural Product Salinipostin A Identifies Essential α/β Serine Hydrolases Involved in Lipid Metabolism in *P. falciparum* Parasites

Euna Yoo,[1,11] Christopher J. Schulze,[1,11] Barbara H. Stokes,[2] Ouma Onguka,[1] Tomas Yeo,[2] Sachel Mok,[2] Nina F. Gnädig,[2] Yani Zhou,[3] Kenji Kurita,[4] Ian T. Foe,[1] Stephanie M. Terrell,[1,5] Michael J. Boucher,[6,7] Piotr Cieplak,[8] Krittikorn Kumpornsin,[9] Marcus C.S. Lee,[9] Roger G. Linington,[4] Jonathan Z. Long,[1,5] Anne-Catrin Uhlemann,[10] Eranthie Weerapana,[3] David A. Fidock,[2,10] and Matthew Bogyo[1,6,12,*]

[1]Department of Pathology, Stanford University School of Medicine, Stanford, CA 94305, USA
[2]Department of Microbiology and Immunology, Columbia University Irving Medical Center, New York, NY 10032, USA
[3]Department of Chemistry, Boston College, Chestnut Hill, MA 02467, USA
[4]Department of Chemistry, Simon Fraser University, Burnaby, BC V5A 1S6, Canada
[5]Stanford ChEM-H, Stanford University, Stanford, CA 94305, USA
[6]Department of Microbiology and Immunology, Stanford University School of Medicine, Stanford, CA 94305, USA
[7]Department of Biochemistry, Stanford University School of Medicine, Stanford, CA 94305, USA
[8]Infectious & Inflammatory Disease Center, Sanford Burnham Prebys Medical Discovery Institute, La Jolla, CA 92037, USA
[9]Wellcome Sanger Institute, Hinxton, Cambridgeshire CB10 1SA, UK
[10]Division of Infectious Diseases, Department of Medicine, Columbia University Irving Medical Center, New York, NY 10032, USA
[11]These authors contributed equally
[12]Lead Contact
*Correspondence: mbogyo@stanford.edu
https://doi.org/10.1016/j.chembiol.2020.01.001

## SUMMARY

**Salinipostin A (Sal A) is a potent antiplasmodial marine natural product with an undefined mechanism of action. Using a Sal A-derived activity-based probe, we identify its targets in the *Plasmodium falciparum* parasite. All of the identified proteins contain α/β serine hydrolase domains and several are essential for parasite growth. One of the essential targets displays a high degree of homology to human monoacylglycerol lipase (MAGL) and is able to process lipid esters including a MAGL acylglyceride substrate. This Sal A target is inhibited by the anti-obesity drug Orlistat, which disrupts lipid metabolism. Resistance selections yielded parasites that showed only minor reductions in sensitivity and that acquired mutations in a PRELI domain-containing protein linked to drug resistance in *Toxoplasma gondii*. This inability to evolve efficient resistance mechanisms combined with the non-essentiality of human homologs makes the serine hydrolases identified here promising antimalarial targets.**

## INTRODUCTION

*Plasmodium falciparum* (*Pf*) is a protozoan parasite that causes the most severe form of human malaria. Malaria threatens 40% of the world's population, resulting in an estimated 228 million cases and nearly 405,000 deaths annually (WHO, 2018). Because of a lack of effective vaccines against the parasite, malaria treatment and control efforts rely on the administration of antimalarial drugs (White et al., 2014). In recent years, artemisinin-based combination therapies (ACTs) have been the first-line antimalarial drugs and have contributed significantly to a reduction in the global malaria burden (Tu, 2011; White, 2008). However, emerging resistance to artemisinin and the partner drugs used in ACTs threatens to reverse the gains that have been made against this disease (Dondorp et al., 2017; van der Pluijm et al., 2019). Therefore, there is a continuing need to identify novel targets and pathways against which efficacious therapeutics can be developed, both to widen the scope of treatment and to overcome existing mechanisms of antimalarial drug resistance.

Natural products have evolved to encompass a broad spectrum of chemical and functional diversity and structural complexity, which enables them to target diverse biological macromolecules in a highly selective fashion. These features of natural products not only suggest that they may hold much promise for the development of therapeutic agents but also make them ideal starting points for the development of chemical probes (Harvey, 2000; Li and Vederas, 2009; Rodrigues et al., 2016; Thomford et al., 2018). Natural product-inspired chemical probes have been instrumental in identifying therapeutic targets and studying poorly understood biological processes and fundamental biology, yet the targets of most natural products remain unknown (Bottcher et al., 2010; Carlson, 2010; Kreuzer et al., 2015; Taunton et al., 1996). Salinipostin A (Sal A) is a natural product produced by a *Salinispora* sp. bacterium. that was isolated from a marine sediment. Sal A displays potent activity against *Pf* parasites, with a half maximal effective concentration ($EC_{50}$) of 50 nM and a selectivity index of >1,000 over a variety of mammalian cell lines (Schulze et al., 2015). In a previous effort to identify drug targets of Sal A, selection experiments were

attempted but failed to generate resistant parasites. These results suggested that Sal A might target multiple proteins or essential pathways for parasite development, and that its potency is not easily compromised by single point mutations. The refractoriness of Sal A to parasite resistance mechanisms combined with its potent and selective activity, and lack of structural similarity to other antimalarials make Sal A an interesting chemical tool to identify druggable pathways in *Pf* parasites.

The α/β hydrolase superfamily is one of the largest groups of structurally related proteins that encompass a diverse range of catalytic activities. Members of this family are composed of largely parallel β sheets flanked on their terminal ends by α helices. The α/β hydrolase domain contains a conserved catalytic dyad or triad formed by a nucleophilic serine residue and an acid-base residue pair. The archetypal α/β hydrolases are esterases, which catalyze two-step nucleophilic substitution reactions to mediate hydrolysis of esters, but substrates for α/β hydrolases also include amides and thioesters (Carr and Ollis, 2009; Holmquist, 2000; Nardini and Dijkstra, 1999; Ollis et al., 1992). In recent years, α/β serine hydrolases have attracted considerable attention for their critical roles in metabolic processes in humans. These metabolic serine hydrolases have been implicated in neurotransmission, pain sensation, inflammation, cancer, and bacterial infection (Bachovchin and Cravatt, 2012; Long and Cravatt, 2011). The *Pf* genome encodes about 40 putative members of the serine hydrolase superfamily based on annotated sequence homologies (Aurrecoechea et al., 2009). However, most of these have not been functionally characterized. Natural product analogs of cyclipostins and cyclophostins, which contain the same reactive functional core electrophile as Sal A, target human and mouse α/β serine hydrolases as well as α/β serine hydrolases involved in lipid metabolism in *Mycobacterium tuberculosis* (Madani et al., 2019; Malla et al., 2011; Nguyen et al., 2017, 2018). These data suggest that α/β hydrolases are promising candidate targets for Sal A in *Pf*.

Activity-based protein profiling (ABPP) has emerged as a powerful and versatile chemical proteomic platform for characterizing the function of enzymes and for rapidly identifying novel targets (Chen et al., 2016; Cravatt et al., 2008; Spradlin et al., 2019; Wright and Sieber, 2016). Central to ABPP is the use of activity-based probes (ABPs), which covalently modify the active sites of enzymes. The bicyclic phosphotriester core in Sal A is hypothesized to form a covalent bond with target proteins upon nucleophilic attack by a catalytic serine or cysteine residue in the target. We therefore devised an analog of Sal A that contains an alkyne group at the terminus of its lipid tail, thereby enabling its use for affinity isolation of labeled target proteins. Herein, we describe the use of this probe to identify multiple essential α/β serine hydrolases, including an essential parasite ortholog of human monoacylglycerol lipase (MAGL) that appears to be one of several targets. We also report that resistance appears to involve mutations in a separate PRELI domain-containing protein that, in *Toxoplasma gondii*, functions as a multidrug resistance mediator (Jeffers et al., 2017). Collectively, our data provide evidence that Sal A inhibits multiple essential serine hydrolases in *Pf*, adversely impacting lipid metabolism, and implicate a new set of metabolic targets for future antimalarial drug discovery and development efforts.

## RESULTS

### Salinipostin A Targets Human and Parasite Depalmitoylases

The Sal A molecule is made up of two parts, namely a reactive cyclic phosphate group that can act as an electrophile for serine and cysteine nucleophiles and a lipid tail that presumably mimics a native cellular lipid. This saturated 15 carbon lipid tail aligns with the 16 carbons in palmitic acid such that the reactive phosphorus is located directly at the site of the carbonyl used to form a thiol ester between palmitate and a cysteine on a palmitoylated protein (Couvertier et al., 2014) (Figure 1A). We therefore reasoned that Sal A might act as a substrate mimetic inhibitor of the serine hydrolases that perform depalmitoylation reactions on proteins (Davda and Martin, 2014; Won et al., 2018). We conducted a competition experiment in which whole *Pf* parasites were incubated with Sal A before labeling with the broad-spectrum serine hydrolase ABP fluorophosphonate-rhodamine (FP-Rho) (Simon and Cravatt, 2010). Several hydrolases were inhibited upon treatment with 1 μM Sal A (Figure 1B). Although palmitoylation is a ubiquitous and dynamic post-translational modification in *Pf* parasites (Corvi et al., 2012; Corvi and Turowski, 2019; Jones et al., 2012), there are no validated depalmitoylases in this parasite. Therefore, we tested Sal A in the related parasite pathogen, *T. gondii*. To determine whether Sal A inhibits the *T. gondii* depalmitoylase PPT1 (TgPPT1), we treated wild-type (WT) (Δku80) and TgPPT1 knockout (ΔPPT1) parasites (Child et al., 2013) with Sal A and labeled parasite extracts with FP-Rho. These studies confirmed that Sal A was able to compete with FP-Rho for labeling of TgPPT1, as well as several other serine hydrolases in *T. gondii* (Figure 1C). Competition studies in human cells (HEK293T) confirmed that Sal A inhibits the human depalmitoylases APT1 and APT2 in a dose-dependent manner, with increased potency against APT2 over APT1 (Figure 1D). In addition, several other less-abundantly labeled human hydrolases were also inhibited by Sal A pretreatment, suggesting that Sal A likely has multiple serine hydrolase targets.

### Synthesis of Salinipostin A Chemical Probe

Because Sal A likely forms covalent bonds with its targets through reaction at the electrophile phosphorus (Figure 2A), this compound was ideally suited to be converted into a probe that could be used to isolate and identify binding proteins in *Pf*. Sal A was originally isolated along with ten analogs, which provided important structure-activity relationship information for the design of the chemical probe. Analysis of these analogs revealed a significant drop in potency against parasites as the length of both the northern alkyl chain (C4>C3>C2) and the western alkyl chain (C15>C14>C13) decreased (Schulze et al., 2015). To minimize structural deviations from the natural product scaffold, we designed a chemical probe with a butyl northern alkyl chain and a terminal alkyne on the western alkyl chain (C16), thus introducing a single carbon and 2 degrees of unsaturation to the parent molecule. Although total syntheses of similar natural products have been accomplished (Malla et al., 2011; Zhao et al., 2018), the bicyclic phosphotriester core of Sal A presents numerous synthetic challenges. Therefore, we opted for a semi-synthetic route in which the natural product Sal A was dealkylated at the western chain and the resulting phosphate diester

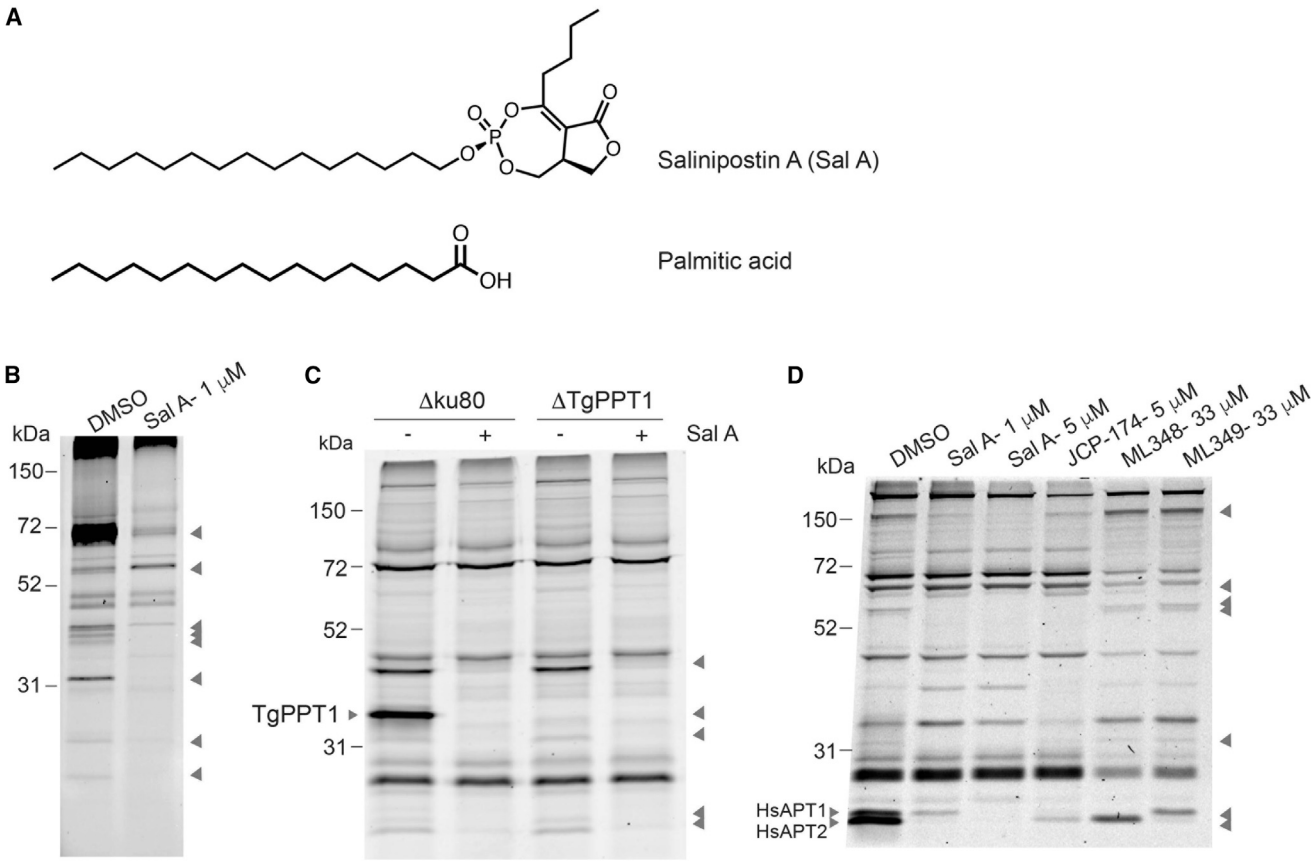


**Figure 1. Sal A Covalently Binds and Inhibits Serine Hydrolases**

(A) Chemical structure of salinipostin A (Sal A) and palmitic acid.

(B–D) Competition assays with the serine hydrolase-reactive fluorophosphonate-rhodamine (FP-Rho) probe identify multiple serine hydrolases as potential targets of Sal A in (B) *Plasmodium falciparum* parasites, (C) *Toxoplasma gondii* Δku80 and ΔPPT1 parasites, and (D) HEK293T cells with or without preincubation with Sal A.

was reacted with an electrophilic alkyne to form two diastereomers of the alkynylated natural product (Sal alk; Figure 2B). Screening of these diastereomers against *Pf* parasites revealed that the isomer corresponding to the parent natural product retained full potency, whereas the other diastereomer showed a 10-fold drop in potency (Figure S1). In addition, we conducted 72 h growth assays in the presence and absence of isopentenyl pyrophosphate (IPP), which is a product of the apicoplast isoprenoid biosynthesis pathway that is essential for growth during the asexual blood stage. An apicoplast-based killing mechanism can be reversed by supplementation of parasite culture medium with IPP (Yeh and DeRisi, 2011). We performed this chemical rescue screen to determine whether the antiplasmodial mechanism of Sal A was related to depletion or disruption of key lipid metabolites derived from the isoprenoid pathway in the apicoplast. The potency of both Sal A and Sal alk was unaffected by IPP, suggesting that these compounds do not target the apicoplast (Figure S1).

## Salinipostin A Targets Multiple Serine Hydrolases in *Pf* Parasites

Having confirmed that Sal alk retained activity equivalent to the parent natural product, we conducted a competition experiment in which parasites were pre-incubated with Sal A for 2 h before Sal alk labeling. CLICK reaction with TAMRA-azide confirmed that Sal alk labeled multiple proteins in *Pf* and that Sal A competed for Sal alk labeling of several of those proteins in a dose-dependent manner (Figure 2C). Therefore, we next used Sal alk as a probe to affinity purify targets of the natural product using a standard ABPP method. For these studies, we pretreated *Pf* parasite cultures with either Sal A or a vehicle control and subsequently labeled cultures with Sal alk. Samples were lysed and labeled proteins were conjugated to biotin-azide using CLICK chemistry. Avidin affinity chromatography was performed to enrich for biotin-azide-labeled proteins. The samples were then subjected to tryptic digestion and tandem mass spectrometry analysis (Table S1). Analysis of these data identified ten putative Sal A targets that were enriched in Sal alk-treated samples and that were correspondingly reduced in Sal A-pretreated samples (Figure 2D; Tables 1 and S1). All ten putative target proteins have $\alpha/\beta$ serine hydrolase domains with either a conserved Ser-His-Asp catalytic triad or a Ser-Asp dyad. Of these, five are annotated as lipases with the characteristic GXSXG motif (http://plasmodb.org/plasmo) (Aurrecoechea et al., 2009). Based on a piggyBac transposon saturation mutagenesis study (Balu et al., 2005,

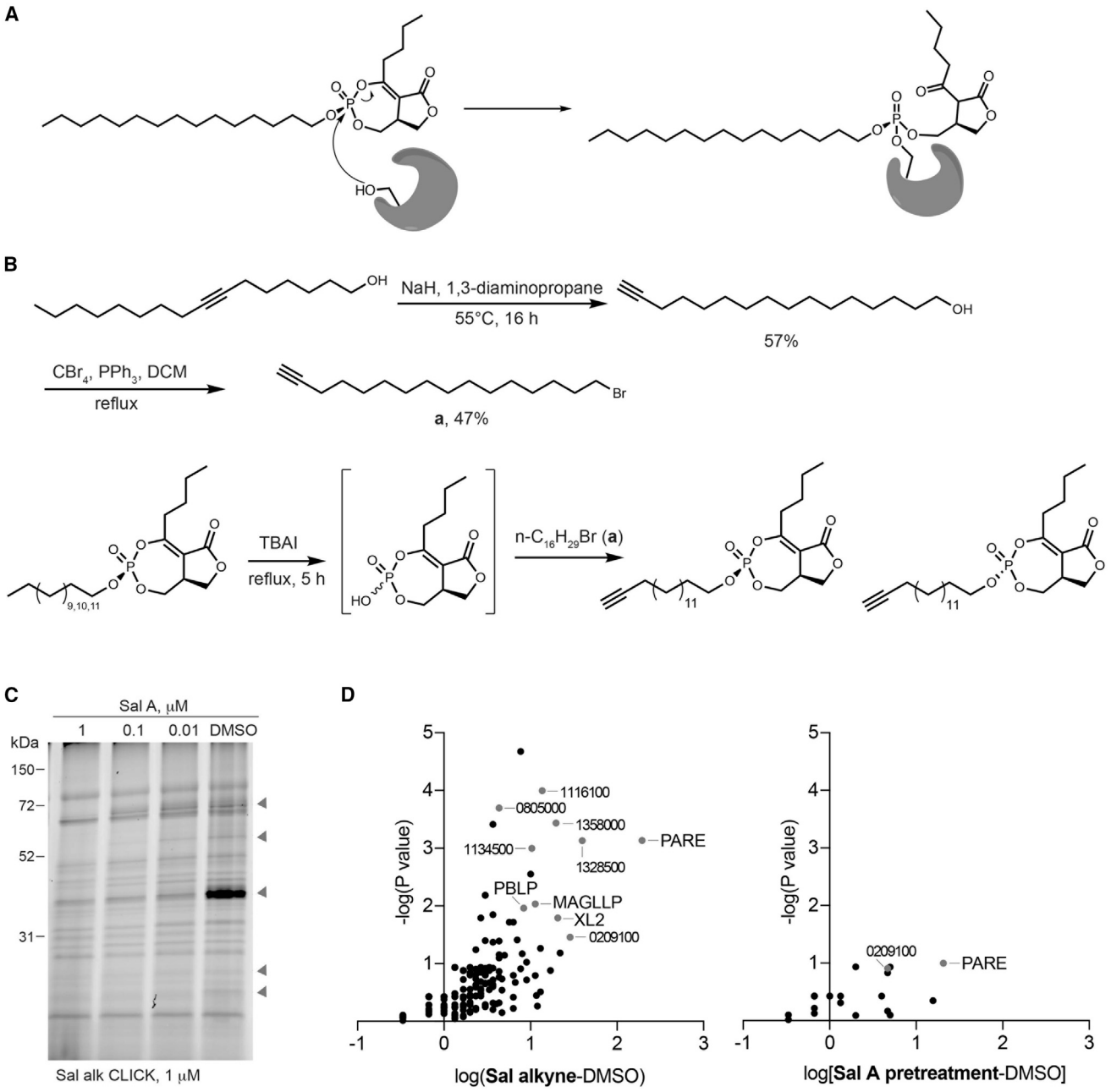


**Figure 2. Sal Alkyne Identifies Multiple Target Proteins in *P. falciparum***

(A) Proposed mode of action of Sal A. This natural product can form a covalent adduct with the nucleophilic serine catalytic residues at the active site of α/β hydrolase enzymes, rendering them inactive.

(B) Semi-synthesis of Sal A alkyne (Sal alk). DCM, dichloromethane; TBAI, tetrabutylammonium iodide (see Figure S1).

(C) Sal alk labeling of proteins in *P. falciparum* with or without Sal A preincubation. After the Sal alk probe labeling, lysates of saponin-isolated parasites were prepared and labeled proteins were conjugated with TAMRA-azide using a CLICK reaction (see Figure S2).

(D) Volcano plots of Sal alk targets in *P. falciparum*. The x axis shows the logarithm values of difference in spectral counts of protein between Sal alk-treated and DMSO vehicle-treated parasites (left) and Sal A-pretreated (competition) and DMSO vehicle-treated parasites (right). The statistical significance was determined without correcting for multiple comparisons in triplicates and the y value in the volcano plot is minus one times the logarithm of the p value. The proteins with high abundance and competition by the parent compound Sal A are highlighted in red (see Tables 1 and S1 for identified proteins in red).

2009; Bushell et al., 2017; Zhang et al., 2018), four of the identified targets are likely to be essential in *Pf*.

One of the proteins identified as a putative Sal A target, PF3D7_1001600 was recently annotated as exported lipase 2 (PfXL2), one of the *Plasmodium* α/β hydrolases containing the export element (PEXEL) motif that is essential for delivery of most exported proteins (Hiller et al., 2004; Marti et al., 2004). Studies with trophozoite/early schizont-stage parasites

**Table 1. Sal A Target Proteins Identified in *P. falciparum***

| Protein ID | Description | MW (kDa) | Essential in *P. falciparum* piggyBac Screen | Spectral Counts |
|---|---|---|---|---|
| PF3D7_0709700 | lysophospholipase (PfPARE) | 42.4 | no | 195.0 |
| PF3D7_1328500 | α/β hydrolase | 115.9 | no | 39.7 |
| PF3D7_0209100 | phospholipase A2 | 78.3 | no | 28.7 |
| PF3D7_1001600 | exported lipase 2 (PfXL2) | 88.6 | yes | 20.7 |
| PF3D7_1358000 | patatin-like phospholipase | 238.2 | no | 19.7 |
| PF3D7_1116100 | serine esterase | 217.1 | no | 13.7 |
| PF3D7_1038900 | esterase, lysophospholipase | 41.8 | yes | 11.3 |
| PF3D7_1134500 | α/β hydrolase | 210.5 | yes | 10.3 |
| PF3D7_0818600 | BEM46-like protein (PBLP) | 34.9 | yes | 8.3 |
| PF3D7_0805000 | α/β hydrolase | 28.5 | no | 4.3 |

expressing a C-terminal GFP fusion of PfXL2 revealed that the protein is exported into the erythrocyte cytosol of parasitized red blood cells (RBCs) (Spillman et al., 2016). Nonetheless, the physiological function of PfXL2 remains unknown, although it is considered to be essential for parasite growth (Bushell et al., 2017; Zhang et al., 2018).

We also identified a *Plasmodium* BEM46-like protein (PBLP, PF3D7_0818600) as another potential target of Sal A. A study of PBLP in the rodent malaria parasite *Plasmodium yoelii* showed that it has an important role in invasion, with deletion of PBLP affecting merozoite formation, sporozoite maturation, and infectivity (Groat-Carmona et al., 2015). The Bud Emergence (BEM) 46 proteins are an evolutionarily conserved class of α/β hydrolases that carry N-terminal signal peptides that can act as transmembrane domains. BEM46 homologs have been implicated in signal transduction and cell polarity (Kumar et al., 2013; Mercker et al., 2009). All *Plasmodium* species appear to express a PBLP ortholog, which suggests a conserved albeit as yet unknown function.

Based on total spectral counts, the most abundantly labeled potential Sal A target was a putative lysophospholipase (PF3D7_0709700). This protein was recently annotated as PfPARE (*P. falciparum* Prodrug Activation and Resistance Esterase), an esterase that is responsible for activating some antimalarial prodrug compounds (Istvan et al., 2017). To test whether PfPARE could be a Sal A target, we obtained *Pf* lines expressing both WT (WT-GFP) and active site mutant (S179T-GFP) PfPARE-GFP fusions replacing the native gene locus. Treatment of these parasites with Sal alk revealed labeling of PfPARE that was dependent on the catalytic serine (Figure S2A). However, parasites expressing the WT or catalytically dead PfPARE were equally sensitive to Sal A treatment (Figure S2B). These results, combined with the predicted lack of essentiality of PfPARE, suggest that it most likely binds Sal A because of its general drug binding properties and that it may not be a relevant target for the compound's parasiticidal action.

## Salinipostin A Inhibits a Monoacylglycerol Lipase-like Protein in *P. falciparum* (PfMAGLLP)

To gain further insight into potential functions of the serine hydrolases that we identified as putative Sal A targets, we performed a sequence homology search and found that three of the ten proteins (PfPARE, PfXL2, and PF3D7_1038900) share sequence similarity with human MAGL (Figures 3A and S3) (Bertrand et al., 2010). It is possible that these proteins all have MAGL-like properties. Unfortunately, we were unable to express and purify PfXL2. A study on PfPARE confirmed its esterase activity and broad substrate specificity. However, the catalytic activity of this enzyme is dispensable for asexual blood stage growth, as active site mutant parasites (S179T) displayed no growth defect (Istvan et al., 2017). The third protein with sequence similarity to human MAGL, PF3D7_1038900, is predicted to encode a hydrolase closely related to PfPARE, with 53% sequence identity over 338 residues. This previously uncharacterized enzyme, referred to henceforth as PfMAGLLP, is predicted to have a common structural core α/β hydrolase fold composed of largely parallel β sheets flanked by α helices. This protein contains the conserved catalytic Ser-His-Asp triad that is characteristic of serine hydrolases (Figures 3B and S4A). Furthermore, the cysteine residue adjacent to the active site that is important for ligand recognition and enzyme activity of human MAGL is conserved in the *Plasmodium* enzyme (Karlsson et al., 1997; Saario et al., 2005).

*In vitro*, human MAGL is capable of hydrolyzing a variety of monoglycerides into free fatty acids and glycerol. This enzyme is responsible for the hydrolytic deactivation of the endocannabinoid 2-arachidonoyl-sn-glycerol (2-AG) and has been implicated in diverse pathophysiological processes, including pain, inflammation, and neuroprotection (Labar et al., 2010; Long et al., 2009). To determine whether the PfMAGLLP is structurally and functionally related to human MAGL, we recombinantly expressed and purified the protein and evaluated its ability to process lipid substrates. PfMAGLLP was able to process various fluorogenic lipid ester substrates bearing different chain lengths including butyrate, octanoate, and monosaturated oleate (Figure 3C). Among the substrates tested, 4-methylumbelliferyl octanoate proved to be an optimal substrate with the highest $k_{cat}/K_m$ value (Figure S4B). PfMAGLLP also efficiently hydrolyzed arachidonoyl-1-thio-glycerol, a close analog of the verified MAGL substrate 2-AG. This substrate produces 1-thioglycerol, which can be subsequently detected by the release of a yellow thiolate ion (TNB) upon reaction with 5,5′-dithiobis(2-dinitrobenzoic acid) (Ellman's reagent, Ellman, 1959) (Figure 3D).

With an active recombinant enzyme and corresponding fluorogenic substrate in hand, we were able to initiate screens for inhibitors of PfMAGLLP. We first tested reported human MAGL

A

```
PF3D7_1038900    MNNLTLGDSNICGTFNKLPFIESYYNRKGILLKSYSWLVKNAIGIIVLVHGLSAHLRLQY
hMAGL            ------------------------------------------------MPEESS------P
                                                                  : .  *

PF3D7_1038900    LKLNVNVVNNDYATLIDADNYYIYEDSWIEEFNKN-------------------------
hMAGL            RRTPQSIPYQDLPHLVNADGQYLFCRYWKPTGTPKALIFVSHGAGEHSGRYEELARMLMG
                  :   .:  :*   *::**. *::   *    . :

PF3D7_1038900    -GYSVYGIDLQGHGESDGLDKLPLHINNFDDYVYDIIDYMRRINNSIVLEKSMQKSTSNK
hMAGL            LDLLVFAHDHVGHGQSEGERMVV---SDFHVFVRDVLQHV--------------------
                  .  *:. *  ***:*:*   :    .:*. :* *:::::

PF3D7_1038900    YTIENREELLPMYLVGLSMGGNIVLRTLEILGKSNEINSNLNIKGCISLAGMISVRMVGS
hMAGL            DSMQKDYPGLPVFLLGHSMGGAIAILTAAERP--G------------HFAGMVLISPLVL
                  ::::    **::*:* **** *.: *       .             :***: :  :

PF3D7_1038900    IDSIKYKYFYLPVMKIFSRYFPTFRPGKKKFKFEKYPFVNDLLFYDK--YRFKGRITNNL
hMAGL            ANPESATTFKVLAAKVLNLVLPNLSLGPIDSSVLSRN-KTEVDIYNSDPLICRAGLKVCF
                  :  . . * : . *::.  :*.:  *  . .. .    .:: :*:.     :. :.  :

PF3D7_1038900    AREILVALDNLHNNIDDIPKNIPILFIHSINDCLGWYEGTVSFYNKLQIDNKELYTLEDM
hMAGL            GIQLLNAVSRVERALP--KLTVPFLLLQGSADRLGDSKGAYLLMELAKSQDKTLKIYEGA
                 . ::* *:..:.. :     .:*:*:::.  * **  :*:  : :  : ::* *   *.

PF3D7_1038900    DHVISME--PGNENVLKKILEWISNLYVQ-------
hMAGL            YHVLHKELPEVTNSVFHEINMWVSQRTATAGTASPP
                  **:  *    .:.*:::*  *:*:  .
```

B

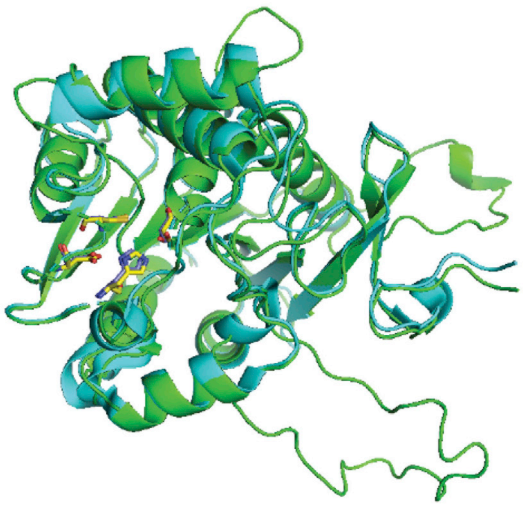

C

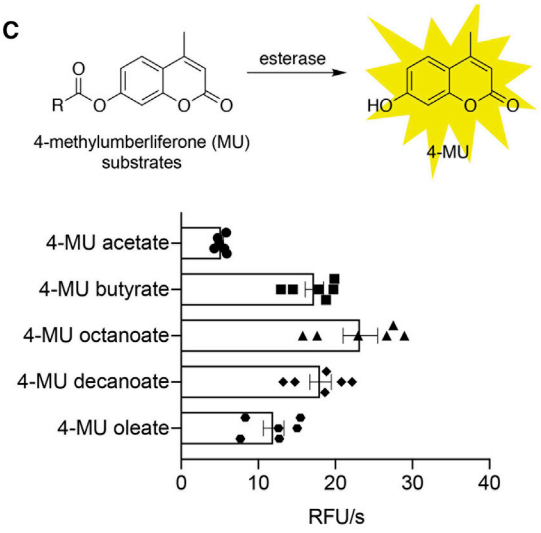


D

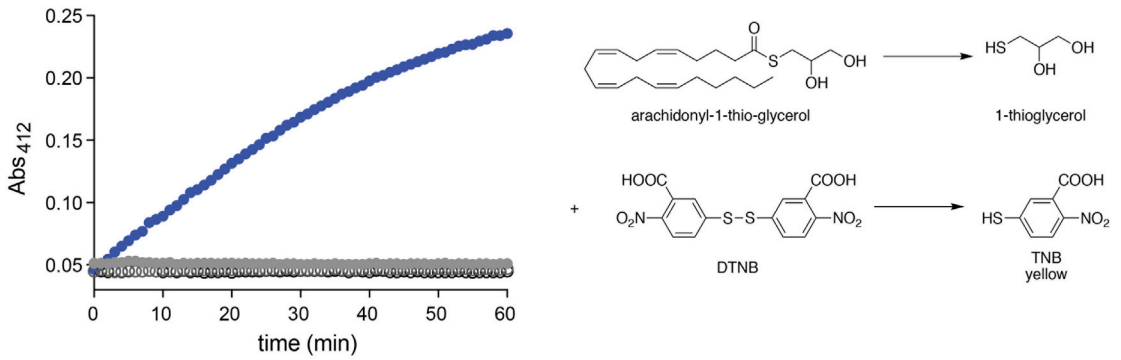


(legend on next page)

inhibitors containing the carbamate electrophile, including KML29, MJN110, JW651, and JZL 184 (Chang et al., 2012, 2013; Niphakis et al., 2013). At 1 μM concentrations, MLN110, JW651, and KML29 inhibited the esterase activity of PfMAGLLP by more than 90%, while JZL 184 inhibited activity by 25%. Dose-response assays showed a broad spectrum of potencies for the four MAGL inhibitors, with $IC_{50}$ (50% inhibitory concentration) values ranging from 2.6 nM for JW651 to 163 nM for KML29 (Figure 4A). JW651 had similar potency against recombinant PfMAGLLP as Sal A, making the compound a useful tool to further explore the function of this enzyme in malaria parasites.

We next performed screening of a small library of 154 serine-reactive triazole-urea-containing compounds and identified 31 hits with greater than 90% inhibition of recombinant PfMAGLLP at 1 μM concentrations (Figure S5A). Further screening of the top 20 most potent hits at lower concentrations identified multiple compounds with strong inhibitory activity in the nM range. These compounds were screened for their ability to compete for active site labeling of PfMAGLLP and human MAGL with the general serine hydrolase probe FP-Rho to identify compounds with the highest potency as well as the greatest selectivity for the parasite enzyme (Figure S5B). All of the top hits showed strong competition for PfMAGLLP; however, some compounds (e.g., AA692, AA691, AA621, and KT165) also bound and blocked labeling of hMAGL at concentrations comparable with the reported hMAGL inhibitor KML29. These compounds were eliminated from further study due to lack of selectivity. We then measured potency of the remaining parasite-specific inhibitors using the original enzyme substrate assay. Although none of triazole-urea hits from the library screen were more potent than Sal A, several had $IC_{50}$ values against the recombinant PfMAGLLP that were in the nanomolar range (Figure 4B). The most active compounds in this series, AA443 and AA642, had $IC_{50}$ values of 15.4 and 7.6 nM, respectively.

To determine whether the potency of inhibition of PfMAGLLP for a given compound correlated with its *in vitro* potency against parasites, we performed dose-response parasite growth inhibition assays with the human MAGL inhibitors and the top triazole-urea hits (Figure 4C). Assays with W2 parasites revealed that the antiplasmodial potencies of this set of compounds largely correlated with the potencies against the recombinant PfMAGLLP enzyme (Figure S6A). The most pronounced exceptions were the compound JW651, which had virtually identical potency as Sal A against recombinant PfMAGLLP, but showed a 16-fold decrease in potency as compared with Sal A against parasites ($EC_{50}$ = 839 versus 50 nM for Sal A), and the compound AA642 that showed strong inhibition against rPfMAGLLP ($IC_{50}$ = 7.6 nM) but reduced potency in inhibiting parasite growth ($EC_{50}$ = 6.3 μM). This discrepancy could be due to reduced cell permeability of JW651 and AA642 or could be the result of Sal A targeting multiple serine hydrolases in the parasite.

We also performed dose-response assays with parasites overexpressing PfMAGLLP from an exogenously transfected plasmid. These parasites showed no apparent shift in Sal A $EC_{50}$ values as compared with WT parasites (Figure S2C). Similar results were obtained for two of the other putative Sal A targets (PF3D7_0808500 and PF3D7_0818600) in that no shift in $EC_{50}$ was observed in parasites exogenously overexpressing these genes. These results suggest that Sal A induces parasite killing by targeting multiple serine hydrolases. However, we still cannot rule out the possibility that other targets of Sal A could be solely responsible for the antiplasmodial activity of the compound.

## Orlistat Is a Potent Inhibitor of PfMAGLLP

Orlistat (Figure 5A), an anti-obesity drug that irreversibly inhibits gastric and pancreatic lipases that hydrolyze triacylglycerols to fatty acids, was also recently found to inhibit the thioesterase domain of fatty acid synthase (Pemble et al., 2007; Weibel et al., 1987). In addition, studies of Orlistat in *Pf* suggest that the compound functions by disrupting parasite neutral lipid metabolism pathways (Gulati et al., 2015).

We tested Orlistat for its ability to inhibit recombinant PfMAGLLP and found that it was equipotent to Sal A, suggesting that this enzyme is a likely target (Figure 5B). Both molecules have similar structures, which include a reactive electrophile that functions by direct covalent modification of the active site serine and blocks binding and processing of lipid substrates. We next performed dose-response assays with Sal A and Orlistat and found that Orlistat is less potent at killing parasites than Sal A ($EC_{50}$ = 280 versus 50 nM for Sal A; Figure 5C). Previously, we reported that both Sal A- and Orlistat-treated parasites showed disorganized internal structures that failed to egress from the infected RBCs (Gulati et al., 2015; Schulze et al., 2015). Fluorescence microscopy imaging of mature schizonts expressing a PfATP-GFP reporter and treated for 18 h with the DMSO vehicle control revealed invagination of the plasma membrane around the individual merozoites during the final stages of cytokinesis and preparation for parasite egress from the infected RBC, as reported previously (Rottmann et al., 2010). In contrast, parasites treated for 18 h with 2 μM Sal A or 6 μM Orlistat showed disorganized plasma membranes that failed to properly surround the merozoites, indicating that both compounds prevented

**Figure 3. PfMAGLLP Is Structurally and Functionally Similar to Human MAGL**

(A) Sequence alignment of PfMAGLLP and hMAGL using Clustal W2. Identical or highly similar residues are indicated with (*) or (:), respectively. Sequence identity is 17% and the fold and function assignment system score is −74.8. The conserved G-X-S-X-G motif and residues of the catalytic triad are highlighted in yellow and cyan, respectively. The cysteine adjacent to the active site is highlighted in green (see Figure S3).

(B) Predicted structure of PfMAGLLP (green) superimposed with human MAGL structure (PDB: 3jw8, cyan) (Bertrand et al., 2010). Catalytic triads are shown in yellow for PfMAGLLP and purple for hMAGL (see Figure S4A).

(C) Processing of 4-methylumbelliferyl (4-MU)-based fluorogenic substrates by recombinant PfMAGLLP. Substrates (10 μM) were incubated with 5 nM of rPfMAGLLP and initial cleavage rates (relative fluorescence units/s) were measured. Data were derived from three independent experiments performed in duplicate and were calculated as non-linear regressions using GraphPad Prism with means ± SD (see Figure S4B).

(D) Hydrolysis of arachidonyl-1-thio-glycerol by rPfMAGLLP. Hydrolysis of the thioester bond by the enzyme generates a free thiol that reacts with 5,5′-dithiobis-(2-nitrobenzoic acid) resulting in a yellow product thionitrobenzoic acid with an absorbance of 412 nm (blue) (Ellman, 1959). In the absence of either enzyme or substrate, there was no absorbance of TNB.

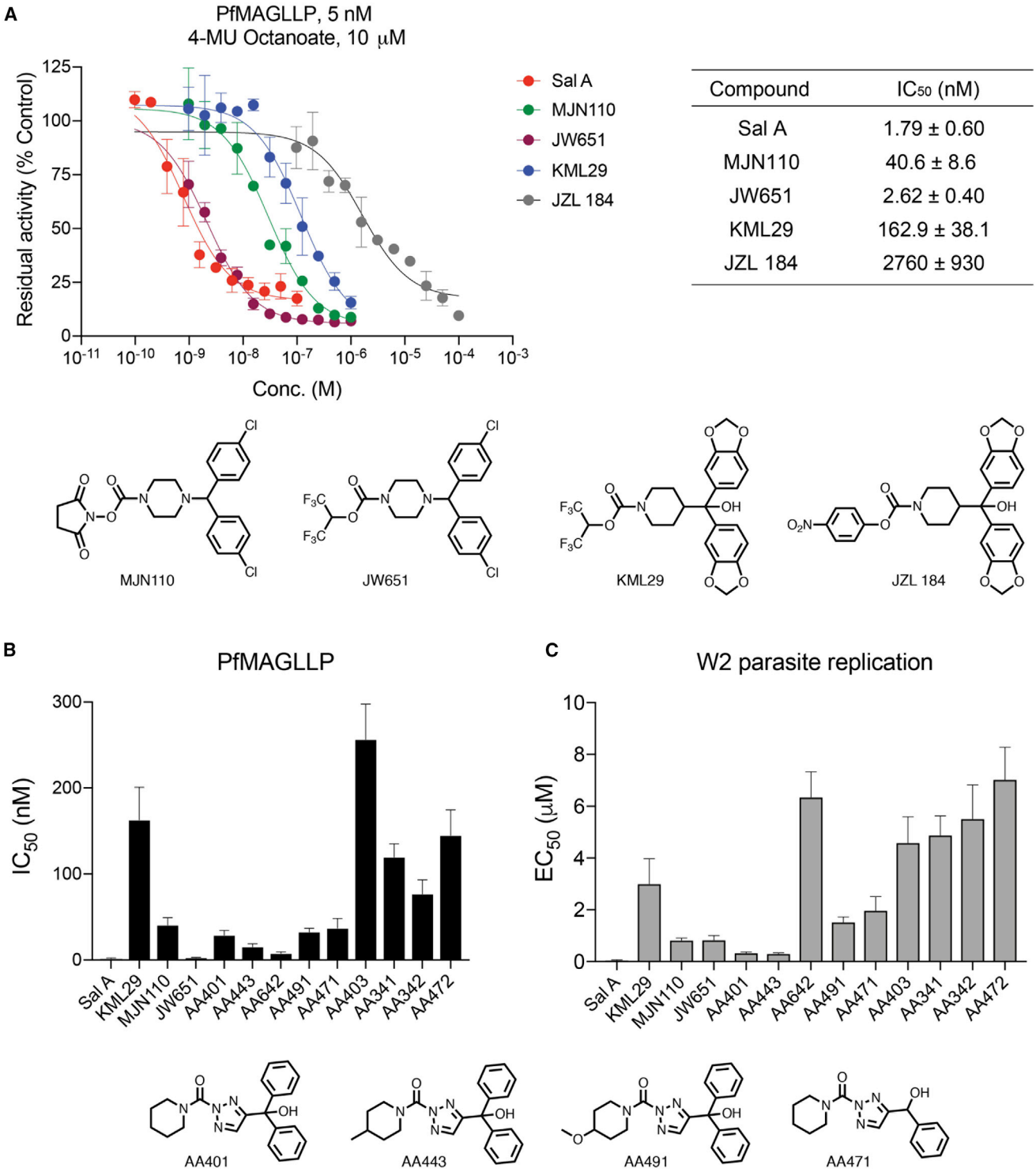


| Compound | $IC_{50}$ (nM) |
|---|---|
| Sal A | 1.79 ± 0.60 |
| MJN110 | 40.6 ± 8.6 |
| JW651 | 2.62 ± 0.40 |
| KML29 | 162.9 ± 38.1 |
| JZL 184 | 2760 ± 930 |

**Figure 4. PfMAGLLP Inhibitor Screening**

(A) Inhibition of rPfMAGLLP as determined by initial cleavage rates (relative fluorescence units/s) by known human MAGL inhibitors (structures shown below). Reactions contained 5 nM rPfMAGLLP and 10 μM 4-methylumbelliferyl octanoate substrate. Data were derived from three independent experiments performed in duplicate and were calculated as non-linear regressions using GraphPad Prism. $IC_{50}$ values are listed (mean ± SD, n = 3).

(B) Inhibition of rPfMAGLLP with a small library of triazole urea-containing compounds (mean ± SD, n = 3, see Figures S5B–S5D).

(C) $EC_{50}$ values of PfMAGLLP inhibitors in 72 h treatment of *P. falciparum* W2 parasites, beginning as synchronized ring stages, with error bars, SD. (n = 6 parasite cultures from two independent experiments with triplicates). Structures of representative compounds are shown (see Figure S6A).

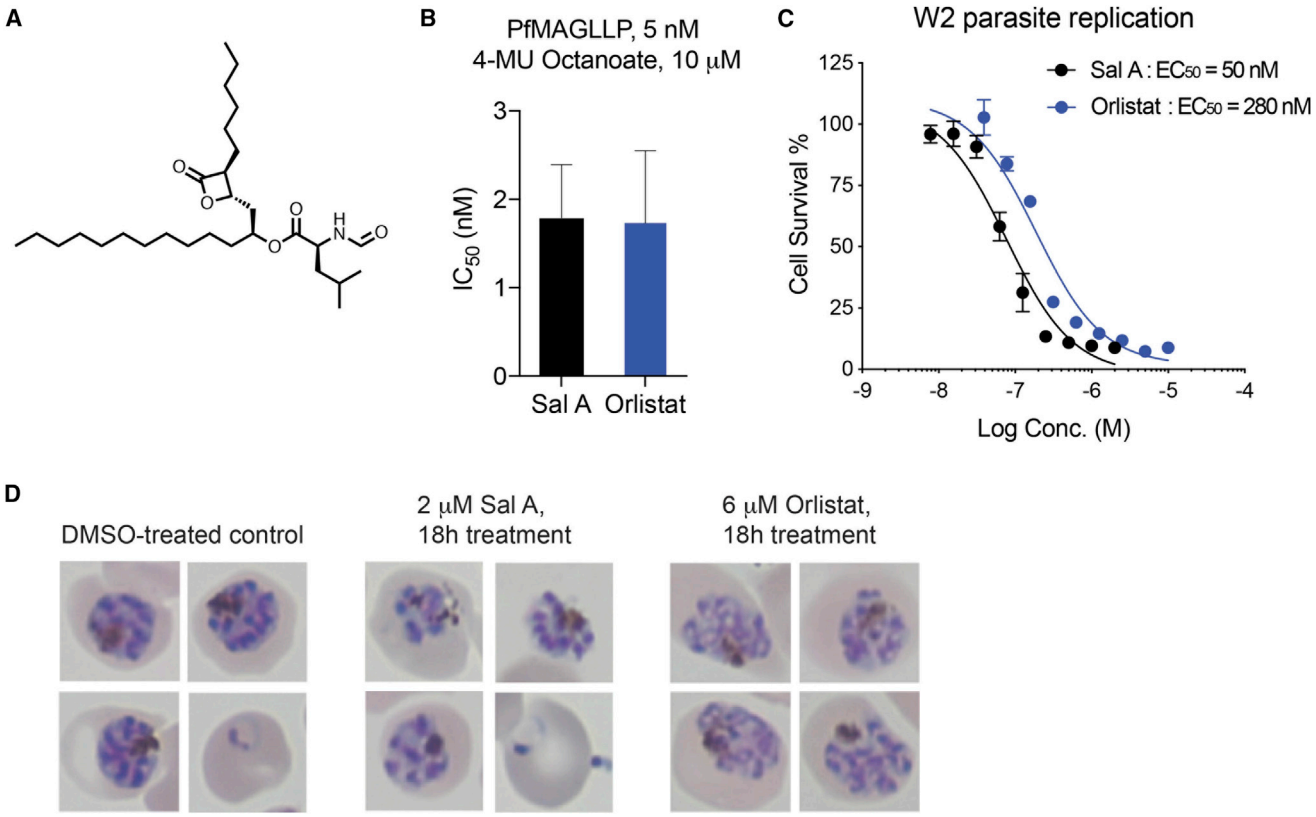


**Figure 5. Effect of Orlistat in Comparison to Sal A**

(A) Chemical structure of Orlistat.

(B) $IC_{50}$ values of Sal A and Orlistat for inhibition of 4-methylumbelliferyl octanoate processing by rPfMAGLLP (mean ± SD, n = 3).

(C) $EC_{50}$ values of Sal A and Orlistat in 72 h treatment of *P. falciparum* W2 parasites, beginning as synchronized ring stages with error bars, SD (n = 6 parasite cultures from three independent experiments with duplicates).

(D) Giemsa-stained parasites. Synchronized trophozoite-stage parasites were treated at 24–30 h post-invasion with DMSO (vehicle control), 2 μM Sal A, or 6 μM Orlistat and imaged 18 h later (see Figure S7).

parasites from completing cytokinesis and egressing from the infected RBCs (Figures 5D and S7).

Based on our results with Orlistat, which showed that the drug functions by blocking key lipid metabolism pathways resulting in accumulation of triacylglycerides (Gulati et al., 2015), we wanted to determine whether similar accumulations of lipid species could be detected in parasites treated with other putative PfMAGLLP inhibitors. We thus performed metabolomic studies on JW651-treated parasites to measure changes in key lipid metabolites. JW651 treatment resulted in an accumulation of monoglycerides, including palmitoyl and oleoyl glycerols, with a greater than 2-fold increase in these products compared with DMSO-treated parasites (Figure S6B). Together, these results suggest that PfMAGLLP has a role in processing these lipid esters, and that Orlistat and JW651 block lipid processing, resulting in schizont arrest and parasite death.

### *In Vitro* Evolution of Resistance to Sal A

Previous attempts at selecting for resistance to Sal A *in vitro* were unsuccessful at generating Sal A-resistant parasites (Schulze et al., 2015). These studies, which subjected $10^{10}$ parasites to 3- to 7-fold $IC_{50}$ concentrations in three separate experiments, yielded no resistant parasites. These selections were performed using W2 WT parasites, and the exposure to low, sublethal concentrations of Sal A (ranging from 160 to 360 nM) allowed a small subset of the parasite population to recrudesce without any demonstrable decrease in sensitivity. To improve our odds of selecting for resistance to Sal A, we made use of a *Pf* parasite line that has two point mutations (D308A and E310A) in DNA polymerase delta (referred to herein as Dd2_Polδ). This polymorphism ablates the polymerase's proofreading (exonuclease) activity, which in *P. berghei* was shown to increase the overall DNA mutation rate (Honma et al., 2014). We performed *in vitro* resistance selections with Sal alk and Dd2_Polδ in duplicate flasks, each containing $1\times10^9$ parasites. Parasites were exposed to 2.5 μM Sal alk (~2× the $IC_{90}$ concentration of Sal alk against the Dd2_Polδ line) over the course of 10 days, after which drug pressure was removed and the cultures were continued in regular medium. Recrudescence was observed microscopically in both flasks at day 17 of the selection. Selected cultures displayed a small but significant shift in $IC_{50}$ when assayed in bulk. Clones from both flasks were obtained by limiting dilution, and six (three from each flask) were selected for whole-genome sequencing analysis. Across the six Sal A-selected clones sequenced, single nucleotide polymorphisms (SNPs) were identified in 44 genes.

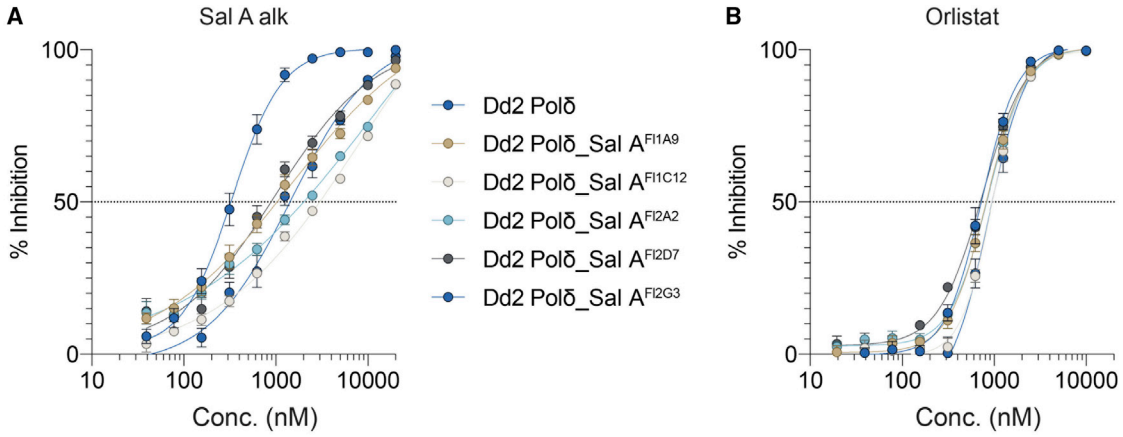


**Figure 6. Sal A-Selected Parasites**

(A and B) Dose-response curves for Sal A-selected parasite clones and the corresponding parental line (Dd2_Polδ) tested against (A) Sal alk or (B) the lipid metabolism inhibitor Orlistat (see Table S2). N,n = 5,2. Data are shown as means ± SEM.

Among these genes, only two showed mutations in clones from both flasks and none of the mutations were in genes coding for α/β hydrolases. Rather, the sole gene that was mutated in all six clones was PF3D7_1324400, which is annotated as a putative PRELI domain-containing protein of unknown function. Five of the six clones harbored a single point mutation in the coding sequence (A20V in clones FI2D7 and FI2G3 from flask 2, or P102L in FI2A2, or T145I from the identical clones FI1C12 and FI1E12 from flask 1; Table S2). The sixth clone, FI1A9, had a point mutation in intron 1 that has an unknown impact on expression levels. The second frequently mutated gene was PF3D7_1235200, encoding a V-type $H^+$-translocating pyrophosphatase, which showed a S725Y mutation in the clones FI1C12 and FI1E12 and an E507K mutation in the clone FI2D7. The absence of mutations in this gene in the other Sal A-resistant clones leads us to suspect that this gene is at best only an occasional contributor to the resistance phenotype and is not the primary determinant. Other mutations arising infrequently are thought to be stochastic events unrelated to the selection pressure.

Drug susceptibility assays with these clones and the parental Dd2_Polδ line showed significant 2- to 9-fold increases in $IC_{50}$ values for the resistant clones (Table S2), with dose-response data showing decreased susceptibility across multiple concentrations (Figure 6A). No significant cross-resistance was observed to Orlistat, known to inhibit the hydrolysis of triacylglycerols in *Pf* (Gulati et al., 2015) (Figure 6B). We also found no cross-resistance to JW651 (Table S2), suggesting different specificities in the modes of action of Sal A and these two other lipid-targeting antimalarials.

## DISCUSSION

Lipid-dependent processes, including the formation of a vacuolar system and the development of daughter cells, play crucial roles in the *Plasmodium* life cycle, and are fueled both by *de novo* synthesis and by acquisition of lipids from the host cell (Ben Mamoun et al., 2010; Vial et al., 2003). Yet the specific enzyme(s) responsible for lipid turnover during the replication and invasion stages of malaria parasites remain poorly understood. Here, we provide evidence that a natural product, Sal A, results in stage-specific inhibition of parasite development by targeting multiple α/β serine hydrolases. This stage-specificity profile is similar to that observed for the anti-obesity drug Orlistat, previously shown to block lipid metabolism pathways in *Plasmodium* parasites (Gulati et al., 2015). One of the primary Sal A targets identified here, PfMAGLLP, demonstrated esterase activity for lipid substrates including monoacylglycerols and was also potently inhibited by Orlistat. Biochemical characterization and inhibitor screening of this hydrolase led to the identification of small-molecule inhibitors that similarly blocked parasite development and led to accumulation of acylglyceride metabolites. Understanding the roles of *Plasmodium* α/β serine hydrolases in host and parasite lipid metabolic networks will likely open up new avenues to discover and develop antimalarials with novel mechanisms of action.

The original studies that identified Sal A as a potent natural product antimalarial postulated that it functioned by disrupting key parasite signaling pathways, and efforts were subsequently made to identify direct targets of the molecule using drug resistance screening (Schulze et al., 2015). These efforts failed to produce resistant mutants and the authors suggested that the compound might kill parasites through pleotropic effects on multiple targets, making it unlikely that resistant mutants could evolve through SNPs. In support of this multi-target hypothesis, studies of the related natural products, cyclipostins and cyclophostins, which contain the same type of phosphate electrophile found in salinipostins, have revealed potent inhibitory activity against multiple classes of serine lipases and esterases. These compounds are also potent against *M.* tuberculosis, and ABPP efforts have identified a number of serine hydrolase targets in that species (Madani et al., 2019; Malla et al., 2011; Nguyen et al., 2017, 2018). A review of the cyclipostins and related compounds suggested that, given the broad-spectrum but class-specific reactivity of the cyclipostins, Sal A might function through inhibition of multiple serine hydrolase targets in *Plasmodium* (Spilling, 2019). We initially hypothesized that Sal A might target serine hydrolases responsible for removing palmitate

from S-palmitoylated proteins, given its structural similarity to palmitic acid. Indeed, we found that Sal A was able to target TgPPT1 and induce a parasite growth and invasion arrest. However, several other serine hydrolases were also effectively targeted by the compound, supporting a generalized mode of action that involves inhibition of multiple enzymes with likely similar catalytic mechanisms and substrates.

Chemical biology has evolved over the past few decades, but a common theme has been the use of small molecules to dissect biological pathways. Although there are examples of small molecules that can be used to perturb specific biological pathways by binding to a single protein target, in many cases, small molecules have effects that are mediated by their ability to interact with multiple protein targets. On the one hand, these types of pleotropic effects make mechanistic studies of small molecules much more challenging, on the other, they make many small molecules useful tools for identifying related proteins that function together in important biological pathways. For Sal A, the results described herein point to a mechanism of action involving disruption of multiple essential serine hydrolases involved in lipid metabolism. Although we were unable to identify which of these hydrolase targets is most integral to the compound's antimalarial activity, likely because parasite killing results from the combined inhibition of several targets, our data identify a number of previously poorly characterized enzymes that, collectively, appear to be essential for parasite survival.

We focused our attention on the three serine hydrolases identified as putative targets of Sal A that have been considered essential in *Pf* based on a recent whole-genome saturation mutagenesis study. Homology searches and predicted structural analyses of these enzymes identified one, PF3D7_1038900, as a likely MAGL protein, due to its sequence homology to the human MAGL involved in processing of acylglycerides and other lipid metabolites. Recombinant expression of this protein, PfMAGLLP, resulted in an active enzyme that was able to process both simple lipid esters as well as a close homolog of the native human MAGL substrate 2-AG. Both Sal A and the anti-obesity drug Orlistat were potent inhibitors of this enzyme. We were also able to identify several novel inhibitors of PfMAGLLP and show that human MAGL inhibitors similarly effectively block its activity. Although we cannot definitively confirm that inhibition of this target by Sal A is the primary cause of parasite killing, we found that the ability of similar compounds to inhibit PfMAGLLP generally correlated with their ability to kill parasites. Furthermore, we observed that a human MAGL inhibitor that is also a potent inhibitor of PfMAGLLP was able to induce accumulation of monoacylglycerides in treated parasites, again linking this enzyme to lipid metabolism in the parasite.

Our efforts to confirm specific serine hydrolases as phenotypically relevant targets of Sal A through drug selection studies resulted in the isolation of parasite clones with moderately diminished sensitivity to the drug. Specifically, we were able to isolate six clones from a putative mutator Dd2 line that showed reproducible reduction in $EC_{50}$ values of approximately 2- to 9-fold as compared with the parental line, and performed whole-genome sequencing on those clones. These data identified 44 genes with point mutations that resulted in either truncation or mutation of predicted protein products. Although this number of mutations is high, the vast majority were found in only one or two of the sequenced clones. Only two genes showed multiple mutations in three or more of the clones and both might thus contribute to general modes of drug resistance. The most likely dominant mediator of the observed reduced sensitivity effect was a gene coding for a PRELI domain-containing protein of unknown function, for which mutations were found in all six clones obtained from both independent flasks. There are multiple examples that distinct mutations in a given gene lead to different levels of resistance (e.g., for the artemisinin resistance determinant *k13*, the chloroquine and piperaquine resistance determinant *pfcrt*, the DDD107498 resistance mediator eEF2 (eukaryotic elongation factor 2), or the DSM265 resistance mediator *dhodh*) (Baragana et al., 2015; Mandt et al., 2019; Ross et al., 2018; Straimer et al., 2015). Our finding that all clones shared a mutation in PF3D7_1324400, following selection of independent culture flasks, provides a very high degree of confidence that variants of this gene are causal for resistance. It is not possible to formally rule out PfPRELID as a target for the antiplasmodial effects of Sal A. However, this protein was not identified in our proteomics studies, nor does it share any chemical properties with any of these $\alpha/\beta$ hydrolases that would suggest the PfPRELID binds Sal A directly. There are well-established instances that antimalarial compounds have separate targets and mechanisms of resistance. Although artemisinin promiscuously targets multiple parasite proteins, lipids, and other biomolecules, the mechanism of resistance appears to be distinct, being driven by separate mutations in a single gene *k13* as a unique survival mechanism that occurs only in very early ring-stage parasites (Tilley et al., 2016; Birnbaum et al., 2020). A study of a non-essential parasite esterase showed that it activates a pepstatin prodrug and acquires mutations that lead to lack of drug activation and parasite resistance (Istvan et al., 2017). Mutations in the ABCI3 transporter mediate resistance phenotypes by affecting the transport of diverse chemotypes with distinct modes of action (Cowell et al., 2018; Murithi et al., 2020).

Although the function of a PRELI domain-containing protein in *Plasmodium* is unclear, a homolog from the related parasite pathogen *T. gondii*, TgPRELID, was recently found to be a mitochondrial protein associated with multidrug resistance (Jeffers et al., 2017). Furthermore, PRELI domain-containing proteins in humans have been implicated in transfer of phospholipids to the inner mitochondrial membrane (Potting et al., 2013). These results suggest that the parasite killing effects of Sal A are pleiotropic, and that point mutations in individual targets are not sufficient to generate resistance. Rather, resistance appears to occur via activation of a general drug resistance pathway in the parasite. Here, our study suggests that compounds with broad-spectrum activity against $\alpha/\beta$ hydrolases constitute exciting leads to develop novel antimalarials that can treat existing multidrug-resistant malarial infections. Future efforts to identify synthetically tractable small-molecule inhibitors of these serine hydrolases in the *Plasmodium* parasite with optimal pharmacokinetic properties will be essential to further validate the serine hydrolases as viable antimalarial drug targets.

## SIGNIFICANCE

**Natural products can be powerful tools to identify novel biological pathways and targets in diverse organisms. Here, we**

**describe functional studies of the marine natural product Sal A, a compound that was discovered as a highly potent and selective antimalarial agent with a poorly defined mechanism of action. Using a semi-synthesis method, we generated a suitably tagged analog of Sal A for target identification studies. Using this probe, we identified a suite of largely uncharacterized serine hydrolases in *P. falciparum* parasites. Several of these enzymes are essential for parasite growth and are likely to be involved in diverse aspects of lipid metabolism and signaling. Our results suggest that the parasite killing effects of Sal A are likely the result of inhibition of multiple serine hydrolases. This mode of action makes generation of resistance through mutations in direct targets difficult. In fact, we found that weak resistance to Sal A was mediated by mutations in a protein linked to multidrug resistance in a related parasite rather than by mutations in target genes. In addition, we found that the antiobesity drug Orlistat induces a phenotypic block in parasite growth that is highly similar to that of Sal A. This drug, which has already been shown to block processing of host-derived lipids, previously had no confirmed targets. At least one of the targets of Sal A is a homolog of human monoacylglycerol lipase (MAGL) and is also potently inhibited by Orlistat, thus linking it to essential lipid metabolism pathways in the parasite. Given the lack of essentiality of many of the human homologs of the identified serine hydrolases coupled with their critical function in parasites, our studies with Sal A have identified a number of poorly characterized enzymes that are attractive targets for new generation antimalarial agents.**

## STAR★METHODS

Detailed methods are provided in the online version of this paper and include the following:



## SUPPLEMENTAL INFORMATION

Supplemental Information can be found online at https://doi.org/10.1016/j.chembiol.2020.01.001.

## ACKNOWLEDGMENTS

We thank Daniel Goldberg for sharing the parasites expressing WT and active site mutant (S179T) PfPARE-GFP fusions. We thank Benjamin Cravatt for providing human MAGL inhibitors and a library of triazole urea-containing compounds. We also thank Ellen Yeh for access to the BD Accuri flow cytometer and helpful discussion. We thank Edgar Deu for his efforts to generate a conditional knockout of PfMAGLLP. We thank Micah Niphakis and Kenneth Lum for the sequence and phylogenetic analysis of serine hydrolases and advice. Funding for this work was provided by NIH NIAID R33 AI127581 (to M.B. and D.A.F.), NIH NIGMS R01GM117004 and R01GM118431 (to E.W.), NIH NIDDK DK105203 and P30DK116074 (to J.Z.L.), and NSERC Discovery (to R.G.L.).

## AUTHOR CONTRIBUTIONS

Conceptualization, E.Y., C.J.S., E.W., and M.B.; Methodology, J.Z.L., A.-C.U., E.W., D.A.F., and M.B.; Formal Analysis, E.Y., C.J.S., B.H.S., T.Y., Y.Z., K. Kurita, P.C., J.Z.L., E.W., D.A.F., and M.B.; Investigation, E.Y., C.J.S., B.H.S., O.O., T.Y., S.M., N.F.G., K. Kurita, K. Kumpornsin, I.T.F., S.M.T., M.J.B., P.C., and E.W.; Writing — Original Draft, E.Y., C.J.S., and, M.B.; Writing — Review & Editing, E.Y., C.J.S., B.H.S., D.A.F., and M.B.; Resources, R.G.L., J.Z.L., A.-C.U., E.W., D.A.F., and M.B.; Supervision, M.C.S.L., E.W., D.A.F., and M.B.; Funding Acquisition, M.C.S.L., R.G.L., J.Z.L., E.W., D.A.F., and M.B.

## DECLARATION OF INTERESTS

The authors declare no competing interests.

Received: October 28, 2019
Revised: December 11, 2019
Accepted: January 3, 2020
Published: January 23, 2020

## REFERENCES

Adibekian, A., Martin, B.R., Chang, J.W., Hsu, K.L., Tsuboi, K., Bachovchin, D.A.S., Speers A.E., Brown, S.J., Spicer, T., Fernandez-Vega, V., et al. (2013). Optimization and characterization of a triazole urea dual inhibitor for lysophospholipase 1 (LYPLA1) and lysophospholipase 2 (LYPLA2) BTI—Probe Reports from the NIH Molecular Libraries Program. Bethesda (MD): National Center for Biotechnology Information (US); 2010-. Available from: https://www.ncbi.nlm.nih.gov/books/NBK133440/.

Adibekian, A., Martin, B.R., Chang, J.W., Hsu, K.L., Tsuboi, K., Bachovchin, D.A.S., Speers A.E., Brown, S.J., Spicer, T., Fernandez-Vega, V., et al. (2014). Characterization of a selective, reversible inhibitor of lysophospholipase 2 (LYPLA2) BTI—Probe Reports from the NIH Molecular Libraries Program. Bethesda (MD): National Center for Biotechnology Information (US); 2010-. Available from: https://www.ncbi.nlm.nih.gov/books/NBK189927/.

Aurrecoechea, C., Brestelli, J., Brunk, B.P., Dommer, J., Fischer, S., Gajria, B., Gao, X., Gingle, A., Grant, G., Harb, O.S., et al. (2009). PlasmoDB: a functional genomic database for malaria parasites. Nucleic Acids Res. *37*, D539–D543.

Bachovchin, D.A., and Cravatt, B.F. (2012). The pharmacological landscape and therapeutic potential of serine hydrolases. Nat. Rev. Drug Discov. *11*, 52–68.

Balu, B., Shoue, D.A., Fraser, M.J., Jr., and Adams, J.H. (2005). High-efficiency transformation of *Plasmodium falciparum* by the lepidopteran transposable element piggyBac. Proc. Natl. Acad. Sci. U S A *102*, 16391–16396.

Balu, B., Chauhan, C., Maher, S.P., Shoue, D.A., Kissinger, J.C., Fraser, M.J., Jr., and Adams, J.H. (2009). piggyBac is an effective tool for functional analysis of the *Plasmodium falciparum* genome. BMC Microbiol. *9*, 83.

Baragana, B., Hallyburton, I., Lee, M.C., Norcross, N.R., Grimaldi, R., Otto, T.D., Proto, W.R., Blagborough, A.M., Meister, S., Wirjanata, G., et al. (2015). A novel multiple-stage antimalarial agent that inhibits protein synthesis. Nature *522*, 315–320.

Basler, M., Mundt, S., Bitzer, A., Schmidt, C., and Groettrup, M. (2015). The immunoproteasome: a novel drug target for autoimmune diseases. Clin. Exp. Rheumatol. *33*, S74–S79.

Ben Mamoun, C., Prigge, S.T., and Vial, H. (2010). Targeting the lipid metabolic pathways for the treatment of malaria. Drug Dev. Res. *71*, 44–55.

Bertrand, T., Auge, F., Houtmann, J., Rak, A., Vallee, F., Mikol, V., Berne, P.F., Michot, N., Cheuret, D., Hoornaert, C., et al. (2010). Structural basis for human monoglyceride lipase inhibition. J. Mol. Biol. *396*, 663–673.

Birnbaum, J., Scharf, S., Schmidt, S., Ernst, J., Hoeijmakers, W.A.M., Flemming, S., Toenhake, C.G., Schmitt, M., Sabitzki, R., Bergmann, B., Fröhlke, U., Mesén-Ramírez, P., Soares, A.B., Herrmann, H., Bártfai, R., and Spielmann, T. (2020). A Kelch13-defined endocytosis pathway mediates artemisinin resistance in malaria parasites. Science *367*, 51–59.

Bottcher, T., Pitscheider, M., and Sieber, S.A. (2010). Natural products and their biological targets: proteomic and metabolomic labeling strategies. Angew. Chem. Int. Ed. *49*, 2680–2698.

Bushell, E., Gomes, A.R., Sanderson, T., Anar, B., Girling, G., Herd, C., Metcalf, T., Modrzynska, K., Schwach, F., Martin, R.E., et al. (2017). Functional profiling of a *Plasmodium* genome reveals an abundance of essential genes. Cell *170*, 260–272.

Carlson, E.E. (2010). Natural products as chemical probes. ACS Chem. Biol. *5*, 639–653.

Carr, P.D., and Ollis, D.L. (2009). Alpha/beta hydrolase fold: an update. Protein Pept. Lett. *16*, 1137–1148.

Chang, J.W., Niphakis, M.J., Lum, K.M., Cognetta, A.B., Wang, C., Matthews, M.L., Niessen, S., Buczynski, M.W., Parsons, L.H., and Cravatt, B.F. (2012). Highly selective inhibitors of monoacylglycerol lipase bearing a reactive group that is bioisosteric with endocannabinoid substrates. Chem. Biol. *19*, 579–588.

Chang, J.W., Cognetta, A.B., Niphakis, M.J., and Cravatt, B.F. (2013). Proteome-wide reactivity profiling identifies diverse carbamate chemotypes tuned for serine hydrolase inhibition. ACS Chem. Biol. *8*, 1590–1599.

Chen, B., Ge, S.-S., Zhao, Y.-C., Chen, C., and Yang, S. (2016). Activity-based protein profiling: an efficient approach to study serine hydrolases and their inhibitors in mammals and microbes. RSC Adv. *6*, 113327–113343.

Child, M.A., Hall, C.I., Beck, J.R., Ofori, L.O., Albrow, V.E., Garland, M., Bowyer, P.W., Bradley, P.J., Powers, J.C., Boothroyd, J.C., et al. (2013). Small-molecule inhibition of a depalmitoylase enhances *Toxoplasma* host-cell invasion. Nat. Chem. Biol. *9*, 651–656.

Corvi, M.M., and Turowski, V.R. (2019). Palmitoylation in apicomplexan parasites: from established regulatory roles to putative new functions. Mol. Biochem. Parasitol. *230*, 16–23.

Corvi, M.M., Alonso, A.M., and Caballero, M.C. (2012). Protein palmitoylation and pathogenesis in apicomplexan parasites. J. Biomed. Biotechnol. *2012*, 483969.

Couvertier, S.M., Zhou, Y., and Weerapana, E. (2014). Chemical-proteomic strategies to investigate cysteine posttranslational modifications. Biochim. Biophys. Acta *1844*, 2315–2330.

Cowell, A.N., Istvan, E.S., Lukens, A.K., Gomez-Lorenzo, M.G., Vanaerschot, M., Sakata-Kato, T., Flannery, E.L., Magistrado, P., Owen, E., Abraham, M., et al. (2018). Mapping the malaria parasite druggable genome by using *in vitro* evolution and chemogenomics. Science *359*, 191–199.

Cravatt, B.F., Wright, A.T., and Kozarich, J.W. (2008). Activity-based protein profiling: from enzyme chemistry to proteomic chemistry. Annu. Rev. Biochem. *77*, 383–414.

Davda, D., and Martin, B.R. (2014). Acyl protein thioesterase inhibitors as probes of dynamic S-palmitoylation. MedChemComm *5*, 268–276.

Dondorp, A.M., Smithuis, F.M., Woodrow, C., and Seidlein, L.V. (2017). How to contain artemisinin- and multidrug-resistant falciparum malaria. Trends Parasitol. *33*, 353–363.

Ekland, E.H., Schneider, J., and Fidock, D.A. (2011). Identifying apicoplast-targeting antimalarials using high-throughput compatible approaches. FASEB J. *25*, 3583–3593.

Ellman, G.L. (1959). Tissue sulfhydryl groups. Arch. Biochem. Biophys. *82*, 70–77.

Garland, M., Schulze, C.J., Foe, I.T., van der Linden, W.A., Child, M.A., and Bogyo, M. (2018). Development of an activity-based probe for acyl-protein thioesterases. PLoS One *13*, e0190255.

Gisselberg, J.E., Dellibovi-Ragheb, T.A., Matthews, K.A., Bosch, G., and Prigge, S.T. (2013). The Suf iron-sulfur cluster synthesis pathway is required for apicoplast maintenance in malaria parasites. PLoS Pathog. *9*, e1003655.

Groat-Carmona, A.M., Kain, H., Brownell, J., Douglass, A.N., Aly, A.S., and Kappe, S.H. (2015). A *Plasmodium* alpha/beta-hydrolase modulates the development of invasive stages. Cell Microbiol. *17*, 1848–1867.

Gulati, S., Ekland, E.H., Ruggles, K.V., Chan, R.B., Jayabalasingham, B., Zhou, B., Mantel, P.Y., Lee, M.C., Spottiswoode, N., Coburn-Flynn, O., et al. (2015). Profiling the essential nature of lipid metabolism in asexual blood and gametocyte stages of *Plasmodium falciparum*. Cell Host Microbe *18*, 371–381.

Harvey, A. (2000). Strategies for discovering drugs from previously unexplored natural products. Drug Discov. Today *5*, 294–300.

Hiller, N.L., Bhattacharjee, S., van Ooij, C., Liolios, K., Harrison, T., Lopez-Estrano, C., and Haldar, K. (2004). A host-targeting signal in virulence proteins reveals a secretome in malarial infection. Science *306*, 1934–1937.

Holmquist, M. (2000). Alpha/beta-hydrolase fold enzymes: structures, functions and mechanisms. Curr. Protein Pept. Sci. *1*, 209–235.

Honma, H., Hirai, M., Nakamura, S., Hakimi, H., Kawazu, S., Palacpac, N.M., Hisaeda, H., Matsuoka, H., Kawai, S., Endo, H., et al. (2014). Generation of rodent malaria parasites with a high mutation rate by destructing proofreading activity of DNA polymerase delta. DNA Res. *21*, 439–446.

Istvan, E.S., Mallari, J.P., Corey, V.C., Dharia, N.V., Marshall, G.R., Winzeler, E.A., and Goldberg, D.E. (2017). Esterase mutation is a mechanism of resistance to antimalarial compounds. Nat. Commun. *8*, 14240.

Jaroszewski, L., Li, Z., Cai, X.-h., Weber, C., and Godzik, A. (2011). FFAS server: novel features and applications. Nucleic Acids Res. *39*, W38–W44.

Jeffers, V., Kamau, E.T., Srinivasan, A.R., Harper, J., Sankaran, P., Post, S.E., Varberg, J.M., Sullivan, W.J., Jr., and Boyle, J.P. (2017). TgPRELID, a mitochondrial protein linked to multidrug resistance in the parasite *Toxoplasma gondii*. mSphere *2*, e00229-16.

Jones, M.L., Tay, C.L., and Rayner, J.C. (2012). Getting stuck in: protein palmitoylation in *Plasmodium*. Trends Parasitol. *28*, 496–503.

Karlsson, M., Contreras, J.A., Hellman, U., Tornqvist, H., and Holm, C. (1997). cDNA cloning, tissue distribution, and identification of the catalytic triad of monoglyceride lipase. Evolutionary relationship to esterases, lysophospholipases, and haloperoxidases. J. Biol. Chem. *272*, 27218–27223.

Kreuzer, J., Bach, N.C., Forler, D., and Sieber, S.A. (2015). Target discovery of acivicin in cancer cells elucidates its mechanism of growth inhibition. Chem. Sci. *6*, 237–245.

Kumar, A., Kollath-Leiss, K., and Kempken, F. (2013). Characterization of bud emergence 46 (BEM46) protein: sequence, structural, phylogenetic and subcellular localization analyses. Biochem. Biophys. Res. Commun. *438*, 526–532.

Labar, G., Wouters, J., and Lambert, D.M. (2010). A review on the monoacylglycerol lipase: at the interface between fat and endocannabinoid signalling. Curr. Med. Chem. *17*, 2588–2607.

Lentz, C.S., Ordonez, A.A., Kasperkiewicz, P., La Greca, F., O'Donoghue, A.J., Schulze, C.J., Powers, J.C., Craik, C.S., Drag, M., Jain, S.K., et al. (2016). Design of selective substrates and activity-based probes for Hydrolase Important for Pathogenesis 1 (HIP1) from *Mycobacterium tuberculosis*. ACS Infect. Dis. *2*, 807–815.

Li, J.W., and Vederas, J.C. (2009). Drug discovery and natural products: end of an era or an endless frontier? Science *325*, 161–165.

Long, J.Z., and Cravatt, B.F. (2011). The metabolic serine hydrolases and their functions in mammalian physiology and disease. Chem. Rev. *111*, 6022–6063.

Long, J.Z., Nomura, D.K., and Cravatt, B.F. (2009). Characterization of monoacylglycerol lipase inhibition reveals differences in central and peripheral endocannabinoid metabolism. Chem. Biol. *16*, 744–753.

Madani, A., Ridenour, J.N., Martin, B.P., Paudel, R.R., Abdul Basir, A., Le Moigne, V., Herrmann, J.L., Audebert, S., Camoin, L., Kremer, L., et al. (2019). Cyclipostins and cyclophostin analogues as multitarget inhibitors that impair growth of *Mycobacterium abscessus*. ACS Infect. Dis. *5*, 1597–1608.

Malla, R.K., Bandyopadhyay, S., Spilling, C.D., Dutta, S., and Dupureur, C.M. (2011). The first total synthesis of (+/–)-cyclophostin and (+/–)-cyclipostin P: inhibitors of the serine hydrolases acetyl cholinesterase and hormone sensitive lipase. Org. Lett. *13*, 3094–3097.

Mandt, R.E.K., Lafuente-Monasterio, M.J., Sakata-Kato, T., Luth, M.R., Segura, D., Pablos-Tanarro, A., Viera, S., Magan, N., Ottilie, S., Winzeler, E.A.A., et al. (2019). *In vitro* selection predicts malaria parasite resistance to dihydroorotate dehydrogenase inhibitors in a mouse infection model. Sci. Transl. Med. *11*, eaav1636.

Marti, M., Good, R.T., Rug, M., Knuepfer, E., and Cowman, A.F. (2004). Targeting malaria virulence and remodeling proteins to the host erythrocyte. Science *306*, 1930–1933.

Mercker, M., Kollath-Leiss, K., Allgaier, S., Weiland, N., and Kempken, F. (2009). The BEM46-like protein appears to be essential for hyphal development upon ascospore germination in *Neurospora crassa* and is targeted to the endoplasmic reticulum. Curr. Genet. *55*, 151–161.

Murithi, J.M., Owen, E.S., Istvan, E.S., Lee, M.C.S., Ottilie, S., Chibale, K., Goldberg, D.E., Winzeler, E.A., Llinas, M., Fidock, D.A., et al. (2020). Combining stage specificity and metabolomic profiling to advance antimalarial drug discovery. Cell Chem. Biol. *27*, 1–14.

Nardini, M., and Dijkstra, B.W. (1999). Alpha/beta hydrolase fold enzymes: the family keeps growing. Curr. Opin. Struct. Biol. *9*, 732–737.

Nguyen, P.C., Delorme, V., Benarouche, A., Martin, B.P., Paudel, R., Gnawali, G.R., Madani, A., Puppo, R., Landry, V., Kremer, L., et al. (2017). Cyclipostins and cyclophostin analogs as promising compounds in the fight against tuberculosis. Sci. Rep. *7*, 11751.

Nguyen, P.C., Madani, A., Santucci, P., Martin, B.P., Paudel, R.R., Delattre, S., Herrmann, J.L., Spilling, C.D., Kremer, L., Canaan, S., et al. (2018). Cyclophostin and cyclipostins analogues, new promising molecules to treat mycobacterial-related diseases. Int. J. Antimicrob. Agents *51*, 651–654.

Niphakis, M.J., Cognetta, A.B., Chang, J.W., Buczynski, M.W., Parsons, L.H., Byrne, F., Burston, J.J., Chapman, V., and Cravatt, B.F. (2013). Evaluation of NHS carbamates as a potent and selective class of endocannabinoid hydrolase inhibitors. ACS Chem. Neurosci. *4*, 1322–1332.

Ollis, D.L., Cheah, E., Cygler, M., Dijkstra, B., Frolow, F., Franken, S.M., Harel, M., Remington, S.J., Silman, I., Schrag, J., et al. (1992). The alpha/beta hydrolase fold. Protein Eng. *5*, 197–211.

Pemble, C.W., Johnson, L.C., Kridel, S.J., and Lowther, W.T. (2007). Crystal structure of the thioesterase domain of human fatty acid synthase inhibited by Orlistat. Nat. Struct. Mol. Biol. *14*, 704–709.

Perez-Riverol, Y., Csordas, A., Bai, J., Bernal-Llinares, M., Hewapathirana, S., Kundu, D.J., Inuganti, A., Griss, J., Mayer, G., Eisenacher, M., et al. (2019). The PRIDE database and related tools and resources in 2019: improving support for quantification data. Nucleic Acids Res. *47*, D442–D450.

Potting, C., Tatsuta, T., König, T., Haag, M., Wai, T., Aaltonen, M.J., and Langer, T. (2013). TRIAP1/PRELI complexes prevent apoptosis by mediating intramitochondrial transport of phosphatidic acid. Cell Metab. *18*, 287–295.

Rodrigues, T., Reker, D., Schneider, P., and Schneider, G. (2016). Counting on natural products for drug design. Nat. Chem. *8*, 531–541.

Ross, L.S., Dhingra, S.K., Mok, S., Yeo, T.A., Wicht, K.J., Kumpornsin, K., Takala-Harrison, S., Witkowski, B., Fairhurst, R.M., Ariey, F., et al. (2018). Emerging Southeast Asian PfCRT mutations confer *Plasmodium falciparum* resistance to the first-line antimalarial piperaquine. Nat. Commun. *9*, 3314.

Rottmann, M., McNamara, C., Yeung, B.K.S., Lee, M.C.S., Zou, B., Russell, B., Seitz, P., Plouffe, D.M., Dharia, N.V., Tan, J., et al. (2010). Spiroindolones, a potent compound class for the treatment of malaria. Science *329*, 1175–1180.

Saario, S.M., Salo, O.M., Nevalainen, T., Poso, A., Laitinen, J.T., Jarvinen, T., and Niemi, R. (2005). Characterization of the sulfhydryl-sensitive site in the enzyme responsible for hydrolysis of 2-arachidonoyl-glycerol in rat cerebellar membranes. Chem. Biol. *12*, 649–656.

Šali, A., and Blundell, T.L. (1993). Comparative protein modelling by satisfaction of spatial restraints. J. Mol. Biol. *234*, 779–815.

Schulze, C.J., Navarro, G., Ebert, D., DeRisi, J., and Linington, R.G. (2015). Salinipostins A-K, long-chain bicyclic phosphotriesters as a potent and selective antimalarial chemotype. J. Org. Chem. *80*, 1312–1320.

Simon, G.M., and Cravatt, B.F. (2010). Activity-based proteomics of enzyme superfamilies: serine hydrolases as a case study. J. Biol. Chem. *285*, 11051–11055.

Spilling, C.D. (2019). The chemistry and biology of cyclophostin, the cyclipostins and related compounds. Molecules *24*, 2579.

Spillman, N.J., Dalmia, V.K., and Goldberg, D.E. (2016). Exported epoxide hydrolases modulate erythrocyte vasoactive lipids during *Plasmodium falciparum* infection. MBio *7*, e01538-16.

Spradlin, J.N., Hu, X., Ward, C.C., Brittain, S.M., Jones, M.D., Ou, L., To, M., Proudfoot, A., Ornelas, E., Woldegiorgis, M., et al. (2019). Harnessing the anti-cancer natural product nimbolide for targeted protein degradation. Nat. Chem. Biol. *15*, 747–755.

Straimer, J., Gnädig, N.F., Stokes, B.H., Ehrenberger, M., Crane, A.A., and Fidock, D.A. (2017). *Plasmodium falciparum* K13 mutations differentially impact ozonide susceptibility and parasite fitness *in vitro*. mBio *8*, e00172-17.

Straimer, J., Gnadig, N.F., Witkowski, B., Amaratunga, C., Duru, V., Ramadani, A.P., Dacheux, M., Khim, N., Zhang, L., Lam, S., et al. (2015). K13-propeller mutations confer artemisinin resistance in *Plasmodium falciparum* clinical isolates. Science *347*, 428–431.

Taunton, J., Collins, J.L., and Schreiber, S.L. (1996). Synthesis of natural and modified trapoxins, useful reagents for exploring histone deacetylase function. J. Am. Chem. Soc. *118*, 10412–10422.

Thomford, N.E., Senthebane, D.A., Rowe, A., Munro, D., Seele, P., Maroyi, A., and Dzobo, K. (2018). Natural products for drug discovery in the 21st century: innovations for novel drug discovery. Int. J. Mol. Sci. *19*, 1578.

Tilley, L., Straimer, J., Gnadig, N.F., Ralph, S.A., and Fidock, D.A. (2016). Artemisinin action and resistance in *Plasmodium falciparum*. Trends Parasitol. *32*, 682–696.

Tu, Y. (2011). The discovery of artemisinin (qinghaosu) and gifts from Chinese medicine. Nat. Med. *17*, 1217–1220.

van der Pluijm, R.W., Imwong, M., Chau, N.H., Hoa, N.T., Thuy-Nhien, N.T., Thanh, N.V., Jittamala, P., Hanboonkunupakarn, B., Chutasmit, K., Saelow, C., et al. (2019). Determinants of dihydroartemisinin-piperaquine treatment failure in *Plasmodium falciparum* malaria in Cambodia, Thailand, and Vietnam: a prospective clinical, pharmacological, and genetic study. Lancet Infect. Dis. *19*, 952–961.

Vial, H.J., Eldin, P., Tielens, A.G., and van Hellemond, J.J. (2003). Phospholipids in parasitic protozoa. Mol. Biochem. Parasitol. *126*, 143–154.

Weerapana, E., Speers, A.E., and Cravatt, B.F. (2007). Tandem orthogonal proteolysis-activity-based protein profiling (TOP-ABPP)—a general method for mapping sites of probe modification in proteomes. Nat. Protoc. *2*, 1414–1425.

Weibel, E.K., Hadvary, P., Hochuli, E., Kupfer, E., and Lengsfeld, H. (1987). Lipstatin, an inhibitor of pancreatic lipase, produced by *Streptomyces*

*toxytricini*. I. Producing organism, fermentation, isolation and biological activity. J. Antibiot. (Tokyo) *40*, 1081–1085.

White, N.J. (2008). Qinghaosu (artemisinin): the price of success. Science *320*, 330–334.

White, N.J., Pukrittayakamee, S., Hien, T.T., Faiz, M.A., Mokuolu, O.A., and Dondorp, A.M. (2014). Malaria. Lancet *383*, 723–735.

WHO. (2018). World Malaria Report 2018 (World Health Organization).

Won, S.J., Cheung See Kit, M., and Martin, B.R. (2018). Protein depalmitoylases. Crit. Rev. Biochem. Mol. Biol. *53*, 83–98.

Wright, M.H., and Sieber, S.A. (2016). Chemical proteomics approaches for identifying the cellular targets of natural products. Nat. Prod. Rep. *33*, 681–708.

Xi, R., Hadjipanayis, A.G., Luquette, L.J., Kim, T.-M., Lee, E., Zhang, J., Johnson, M.D., Muzny, D.M., Wheeler, D.A., Gibbs, R.A., et al. (2011). Copy number variation detection in whole-genome sequencing data using the Bayesian information criterion. Proc. Natl. Acad. Sci. U S A *108*, E1128.

Yeh, E., and DeRisi, J.L. (2011). Chemical rescue of malaria parasites lacking an apicoplast defines organelle function in blood-stage *Plasmodium falciparum*. PLoS Biol. *9*, e1001138.

Zhang, M., Wang, C., Otto, T.D., Oberstaller, J., Liao, X., Adapa, S.R., Udenze, K., Bronner, I.F., Casandra, D., Mayho, M., et al. (2018). Uncovering the essential genes of the human malaria parasite *Plasmodium falciparum* by saturation mutagenesis. Science *360*, eaap7847.

Zhao, M., Wei, X., Liu, X., Dong, X., Yu, R., Wan, S., and Jiang, T. (2018). Total synthesis of marine cyclic enol-phosphotriester salinipostin compounds. J. Ocean Univ. China *17*, 683–689.

## STAR★METHODS

### KEY RESOURCES TABLE

| REAGENT or RESOURCE | SOURCE | IDENTIFIER |
|---|---|---|
| Antibodies | | |
| Living Colors® Full-Length GFP Polyclonal Antibody | Takara (formerly Clontech) | Cat# 632592; RRID: AB_2336883 |
| Bacterial and Virus Strains | | |
| *E. coli* BL21DE3 | New England Biolabs | Cat# C2527 |
| Chemicals, Peptides, and Recombinant Proteins | | |
| Recombinant *P. falciparum* PfMAGLLP | This paper | N/A |
| Recombinant human monoacylglycerol lipase (MAGL) | Cayman Chemical | Cat# 10007812 |
| Salinipostin A | (Schulze et al., 2015) | N/A |
| JCP174 | (Child et al., 2013) | N/A |
| ML348 | (Adibekian et al., 2014) | N/A |
| ML349 | (Adibekian et al., 2014) | N/A |
| JZL 184 | Cayman Chemical | Cat# 13158 |
| JW651 | Sigma-Aldrich | Cat# SML0990 |
| MJN110 | (Niphakis et al., 2013) | N/A |
| KML29 | (Chang et al., 2012) | N/A |
| Trialzole urea library | Benjamin Cravatt Laboratory (Adibekian et al., 2013) | N/A |
| Orlistat | Cayman Chemical | Cat#10005426 |
| Fluorophosphonate-rhodamine (FP-Rho) | (Lentz et al., 2016) | N/A |
| 7-Acetoxy-4-methylcoumarin | Santa Cruz Biotech. | Cat# sc-206060 |
| 4-Methylumbelliferyl butyrate | Santa Cruz Biotech. | Cat# sc-206912 |
| 4-Methylumbelliferyl caprylate | Santa Cruz Biotech. | Cat# sc-281420 |
| 4-Methylumbelliferyl decanoate | Santa Cruz Biotech. | Cat# sc-206913 |
| 4-Methylumbelliferyl oleate | Santa Cruz Biotech. | Cat# sc-206915 |
| Arachidonoyl-1-thio-glycerol | Cayman Chemical | Cat# 10007904 |
| 5,5′-Dithiobis(2-nitrobenzoic acid) | Sigma-Aldrich | Cat# D8130 |
| YOYO-1 iodide | Thermo Fisher | Cat# Y3601 |
| Critical Commercial Assays | | |
| BCA protein assay kit | Pierce | Cat# 23225 |
| Deposited Data | | |
| Crystal structure of human monoacylglycerol lipase | (Bertrand et al., 2010) | PDB: 3jw8 |
| Mass spectrometry proteomics (PRIDE) | This paper | PXD016835 |
| Experimental Models: Cell Lines | | |
| HEK293T cells | ATCC | ATCC CRL-3216 |
| Experimental Models: Organisms/Strains | | |
| *T. gondii* strain ΔKu80 | (Child et al., 2013) | N/A |
| *T. gondii* strain ΔKu80Δppt1 | (Child et al., 2013) | N/A |
| *P. falciparum* strain W2 | MR4 | N/A |
| *P. falciparum* strain WT PfPARE-GFP | (Istvan et al., 2017) | N/A |
| *P. falciparum* strain S179G PfPARE-GFP | (Istvan et al., 2017) | N/A |
| *P. falciparum* strain Dd2_Polδ | This paper | N/A |
| Software and Algorithms | | |
| Modeller | (Šali and Blundell, 1993) | https://salilab.org/modeller/ |
| FFAS (Fold & Function Assignment) program | (Jaroszewski et al., 2011) | http://ffas.godziklab.org/ffas-cgi/cgi/document.pl |

(*Continued on next page*)

*Continued*

| REAGENT or RESOURCE | SOURCE | IDENTIFIER |
|---|---|---|
| PYMOL | The PyMOL Molecular Graphics System, Schrodinger, LLC | https://pymol.org/ |
| GraphPad Prism | GraphPad Software Inc | https://www.graphpad.com/scientific-software/prism/ |

## LEAD CONTACT AND MATERIALS AVAILABILITY

Further information and requests for resources and reagents should be directed to and will be fulfilled by the Lead Contact, Matthew Bogyo (mbogyo@stanford.edu). We may require a payment and/or a completed Materials Transfer Agreement if there is potential for commercial application.

## EXPERIMENTAL MODEL AND SUBJECT DETAILS

### *Toxoplasma gondii* Parasite Culture

Parasites were grown in human foreskin fibroblasts (HFFs) using a mixture of Dulbecco's modified Eagle's medium (DMEM) with 10% FetalPlex animal serum complex (Gemini Biotech, catalog no. 100602), 2 mM l-glutamine, 100 μg/ml penicillin, and 100 μg/ml streptomycin. Parasites were cultured at 37°C in 5% $CO_2$.

### *Plasmodium falciparum* Parasite Culture

*P. falciparum* W2 and Dd2_Polδ cultures were maintained, synchronized, and lysed as previously described (Straimer et al., 2017). Parasite cultures were grown in human erythrocytes (no blood type discrimination) purchased from the Stanford Blood Center (approved by Stanford University) or the Interstate Blood Bank (for Columbia University).

## METHOD DETAILS

### *P. falciparum* Replication Assays

Ring stage *P. falciparum* culture at 1% parasitemia and 0.5% hematocrit was added to 96-well plates spotted with compounds. The *P. falciparum* culture was incubated with each compound for 72 h. After incubation, the culture was fixed in a final concentration of 1% paraformaldehyde (in PBS) for 30 min at room temperature. The nuclei stain YOYO-1 was then added to a final concentration of 50 nM and incubated overnight at 4°C. Parasite replication was monitored by observation of a YOYO-1-positive population (infected) and YOYO-1-negative population (uninfected) using a BD Accuri C6 automated flow cytometer.

### FP-rho Labeling Competition Assays

*Plasmodium* parasites (ring/troph, 13% parasitemia) were treated with either DMSO or Sal A for 3 h at 37°C. Cultures were centrifuged and RBCs were saponin-lysed (0.15%). Parasite pellets were washed with PBS and lysed in lysis buffer (50 mM Tris, pH 7.4, 150 mM NaCl, 0.5% NP40, 0.1% SDS) for 30 min on ice. Intact *T. gondii* parasites and HEK 293T cells were treated as previously described (Garland et al., 2018). Lysates were then clarified by centrifugation at 4°C, and the protein concentration was quantified using BCA. 50 μg lysate was incubated with 1 μM FP-rho for 1 h at 37°C. Reactions were quenched with reducing SDS sample buffer, and then the entire reaction was resolved by SDS-PAGE. Typhoon flat-bed scanner was used to scan the gel (532-nm laser, 610-nm filter, PMT700). Where necessary, the gel was then Western blotted.

### Salinipostin Alkyne Labeling

*Plasmodium* parasites (ring/troph, 13% parasitemia) were treated with either DMSO or Sal A for 2 h at 37°C, followed by Sal alkyne labeling for 2 h at 37°C with light rocking. Pellets were prepared and lysed as described above. Click labeling was performed by adding 50 μg of membrane lysate in 44 μL of total volume with PBS. Add 1 μL of 50 mM $CuSO_4$, 1 μL 50 mM TCEP, 3 μL of 1x ligand (Tris [(1-benzyl-1H-1,2,3-triazol-4-yl)methyl]amine (Sigma-Aldrich) 20% DMSO in *t*-butanol, final of 100 μM), and 1 μL of 1 mM Rhodamine-azide. Samples were then vortexed, incubated for 30 min, and that procediure repeated. SDS gel loading buffer was then added and SDS-PAGE performed. Gel fluorescecnce was then scanned as above.

### Sample Preparation and Liquid Chromatography–Mass Spectrometry (LC-MS) Analysis for Proteomics

*P. falciparum* W2 cultures (3 x 125 mL) were grown to 23% parasitemia at a ratio of 1:1 rings:trophozoites, and treated with either vehicle (DMSO), 1 μM Sal alk, or 1 μM Sal A, for 2 h at 37°C with slow shaking. For the 1 μM Sal A treatment, 1 μM Sal alk was added after the initial 2 h incubation and the flask was returned to the incubator for an additional 2 h. Parasites were harvested by saponin lysis. Parasite pellets were lysed in 50 mM TEOA, 4% SDS, 150 mM NaCl, pH 7.4 and quantified. Two milligrams of total protein per

technical replicate (n=3) was subjected to a Click reaction in 500 μL total volume by addition of 20 μL $CuSO_4$, 60 μL TBTA, 20 μL 5 mM biotin azide, and 20 μL TCEP and rotating at room temperature for 2.5 h. Samples were prepared for LC-MS analysis as described previously (Weerapana et al., 2007).

### Expression, Purification of Recombinant PfMAGLLP

A codon-optimized version of the PF3D7_1038900 gene was purchased from IDT (Integrated DNA Technologies Inc., San Diego, CA, USA). After cloning into the expression vector pET-28a, the protein contained an N-terminal hexa-His tag. Proteins were expressed in BL21-CodonPlus (DE3)-RIL *Escherichia coli* (Agilent Technologies, catalog no. 230245) at 37°C with 0.25 mM IPTG (Isopropyl β-D-1-thiogalactopyranoside) for 4 h. Recombinant proteins were purified as previously described (Child et al., 2013) with the following modifications: 0.02% NP-40 detergent and 10% glycerol were included in both the lysis and wash buffer. Protein concentrations were quantitated by bicinchoninic acid (BCA) assay.

### Structure Prediction and Modeling of PfMAGLLP

The homology model building comprised two steps: finding best structural template by performing sequence alignment of a target sequence with sequences of proteins, for which experimental structure was known, and then applying modeling program that built a three-dimensional model satisfying spatial constraints of the template structure. We applied FFAS (Fold & Function Assignment) program (Jaroszewski et al., 2011) for the alignment against PDB structures and Modeller software (Šali and Blundell, 1993) for building the model structures.

### Fluorogenic Substrate Assays

10 μL of a rPfMAGLLP solution (5 nM) in PBS containing 0.05% Triton X-100, 1 mM DTT was added to the wells of a black flat-bottom 384-well plate. Stock solutions of 4-methylumbelliferyl (4-MU)-based fluorogenic substrates were dissolved in DMSO (1 mM) and diluted in assay buffer. 10 μL of substrates was added and fluorescence (λex = 365 nm and λem = 455 nm) was read at 37°C in 1 min intervals on a Cytation 3 imaging reader (BioTek, Winooski, VT, USA) for 60 min. Turnover rates in the linear phase of the reaction were calculated using as RFU/sec. For inhibitor screening, the compounds were pre-incubated with enzyme for 30 min at room temperature prior to the addition of substrate.

### Monoacylglycerol Lipase Assay

To a 199 μL of enzyme (50 nM) in 10 mM Tris, 1 mM EDTA, pH 7.4 in an opaque flat-bottom 96-well plate we added 0.5 μL of arachidonoyl-1-thio-glycerol 25 mM (final concentration of 62.5 μM) and 1 μL of DTNB 25 mM (final concentration of 125 μM). The plate was carefully shaken for 10 sec and absorbance was read at 412 nm for 45 min at room temperature.

### FP-Rho Labeling of rPfMAGLLP and Human MAGL

rPfMAGLLP or human MAGL (50 nM) in PBS with 1 mM DTT were preincubated with different concentrations of compounds or DMSO for 30 min at room temperature, before FP-Rho (1 μM) was added. Samples were incubated at room temperature for 30 min, boiled in SDS loading buffer and analyzed by SDS-PAGE.

### Generation of Overexpressing Parasites (pLN and pRL2)

Pf_0818600, Pf_1038900, or Pf_0805000 were synthesized as GeneBlocks (Basler et al., 2015) and cloned in pLN and pRL2 plasmids containing an HA tag and transfected as previously described (Gisselberg et al., 2013) using the Bxb1 mycobacteriophage integrase system in Dd2 parasites containing the attB recombination site in combination with a red blood cell (RBC) preloading technique. Successful integration was confirmed by PCR and Western blot.

### Generation of Dd2_Polδ Parasites

Dd2 parasites with a mutated DNA polymerase δ subunit were generated by CRISPR/Cas9 editing. The mutations, D308A and E310A, were selected based on published work in *P. berghei* (Honma et al., 2014). Briefly, a donor of 658 bp was designed that introduced these two point mutations, as well as additional silent mutations at the gRNA sites. Two gRNAs were designed (gRNA1: AAGGATAAAATTCTTAACTT; gRNA2: TGTATAAAATTAGACGGTAA). The Cas9, gRNAs, and donor sequences were cloned into the plasmid pDC2-cam-coCas9-U6.2-hDHFR. Parasites transfected into this plasmid were selected with 2.5 nM WR99210 for 8 days, followed by removal of selection pressure. Transfectants were genotyped to confirm editing and cloned by limiting dilution.

### Imaging of PfATP4-GFP Parasites

Sorbitol-synchronized parasites expressing the parasite plasma membrane protein PfATP4 fused to GFP (Rottmann et al., 2010), were treated at 24-30 hours post-invasion (hpi) with either 2 μM Sal A, 6 μM Orlistat or DMSO (control), and cultured for an additional 18 h. Cells were then harvested and fixed in 4% v/v formaldehyde supplemented with 0.0075% v/v glutaraldehyde (Sigma) in 1×PBS for 30 min at room temperature. Cell membranes were permeabilized in 0.1% Triton X-100 in PBS for 30 min and autofluorescence was quenched using 0.1 M glycine in PBS for 15 min. Blocking was performed with 3% w/v bovine serum albumin (BSA) for 1 h at room temperature. Cells were incubated with anti-GFP (Clonetech; 1:200 dilution in 3% BSA and 0.1% Tween in PBS) for 90 min at room temperature, and for 60 min with an anti-rabit Alexa Fluor™ 488-conjugated secondary antibody (ThermoFisher,

1:2000 dilution in 3% BSA and 0.1% Tween in PBS). Thin blood smears of stained RBCs were prepared on microscope slides and mounted with cover slips using Prolong Diamond Antifade Mountant with DAPI (ThermoFisher). Slides were imaged using a Nikon Eclipse Ti-E wide-field microscope equipped with an sCMOS camera (Andor) and a Plan Apochromate oil immersion objective with 100× magnification (1.4 numerical aperture). A minimum of 20 Z-stacks (0.2 μm step size) were taken of each parasitized RBC. NIS-Elements imaging software (Version 5.02, Nikon) was used to deconvolve images and perform 3D-volume reconstructions. Deconvolution was performed using 25 iterations of the Richardson-Lucy algorithm for each image.

### Sample Preparation for Lipidomics

*P. falciparum* W2 cultures were maintained in human RBCs in RPMI 1640 complete medium and synchronized with 5% D-sorbitol (w/v) for two or more successive growth cycles and expanded to 8-10% parasitemia prior to harvesting. For lipid analysis, 75 ml cultures were prepared at 8-10% parasitemia and 4-6% hematocrit. Cultures were treated with or without 6.4 μM JW651 (8 × $EC_{50}$) at 8 hpi (triplicate cultures of one bioreplicate). Parasites were monitored by blood smears and harvested at 48 hpi while drugs were maintained until the final time point. The medium was removed and cells were resuspended in 1.5 ml of PBS buffer and transferred into glass vials pre-loaded with 2:1 $CHCl_3$:MeOH to final ratio of 2:1:1 $CHCl_3$:MeOH:PBS. Samples were shaken and centrifuged at 1000 RPM for 5 min at 4°C. The bottom layer was pulled into a new glass vial and dried under nitrogen gas flow. Samples were then analyzed on Q-TOF.

### Analysis of Lipids Using High-Performance Liquid Chromatography-Mass Spectrometry

Mass spectrometry analysis was performed with an electrospray ionization (van der Pluijm et al., 2019) source on an Agilent 6545 Q-TOF LC/MS in positive and negative ionization modes. For Q-TOF acquisition parameters, the mass range was set from 100 to 1200 m/z with an acquisition rate of 10 spectra/second and time of 100 ms/spectrum. For Dual AJS ESI source parameters, the drying gas temperature was set to 250°C with a flow rate of 12 l/min, and the nebulizer pressure was 20 psi. The sheath gas temperature was set to 300°C with a flow rate of 12 l/min. The capillary voltage was set to 3500 V and the fragmentor voltage was set to 100 V. For separation of nonpolar metabolites, reversed-phase chromatography was performed with a Luna 5 μm C5 100 Å LC column (Phenomenex cat # 00B-4043-E0). Samples were injected at 20 μl each. Mobile phases for positive ionization mode acquisition were as follows: Buffer A, 95:5 water/methanol with 0.1% formic acid; Buffer B, 60:35:5 isopropanol/methanol/water with 0.1% formic acid. Mobile phases for negative ionization mode acquisition were as follows: Buffer A, 95:5 water/methanol with 0.1% ammonium hydroxide; Buffer B, 60:35:5 isopropanol/methanol/water with 0.1% ammonium hydroxide. All solvents were HPLC-grade. The flow rate for each run started with 0.5 minutes 95% A / 5% B at 0.6 ml/min, followed by a gradient starting at 95% A / 5% B changing linearly to 5% A / 95% B at 0.6 ml/min over the course of 19.5 minutes, followed by a hold at 5% A / 95% B at 0.6 ml/min for 8 minutes and a final 2 minutes at 95% A / 5% B at 0.6 ml/min. The raw Agilent .d files were converted to mzXML format using MSConvert and then imported into XCMS software to identify features specifically differentially regulated in drug-treated versus vehicle-treated samples. The following XCMS parameters were used: step = 0.05, mzdiff = 0.05, snthresh = 5, mzwid = 0.1.

### *In Vitro* Evolution of Drug-Resistant Lines

To select for Sal A-resistant parasites, duplicate flasks of $1\times10^9$ Dd2_Polδ parasites, each with a starting parasitemia below 2%, were exposed to Sal alk at a concentration of 2.5μM (~2× the $IC_{90}$ concentration). Drug-containing media was refreshed every other day for the first ten days, after which drug pressure was removed and cultures were continued in drug-free medium. Recrudescence was monitored microscopically.

### DNA Library Preparation and Whole Genome Sequencing

200 ng of genomic DNA was used to prepare DNA sequencing libraries using the Illumina Nextera DNA Flex library prep kit with dual indices. The samples were multiplexed and sequenced on an Illumina MiSeq to obtain 300 base-pair paired-end reads at an average of 50× depth of coverage. Sequence reads were aligned to the *P. falciparum* 3D7 genome (PlasmoDB version 36) using Burrow-Wheeler Alignment (BWA). PCR duplicates and unmapped reads were filtered out using Samtools and Picard. Reads were realigned around indels using GATK RealignerTargetCreator and base quality scores were recalibrated using GATK BaseRecalibrator. GATK HaplotypeCaller (version 3.8) was used to identify all SNPs in the resistant clones. SNPs were filtered based on quality scores (variant quality as function of depth QD > 1.5, mapping quality > 40, min base quality score > 18) and read depth (depth of read > 5) to obtain high quality SNPs. These SNPs were annotated using snpEFF. Comparative SNP analyses between the resistant clones and the parental Dd2_Polδ line were performed to generate a final list of SNPs that were present exclusively in the resistant clones. Integrated genome viewer (IGV) was used to visually verify the presence of these SNPs in the clones. BIC-Seq (Xi et al., 2011) was used to check for copy number variations (CNVs) in the resistant mutants using the Bayesian statistical model. CNVs in highly variable surface antigens and multi-gene families were removed as these are prone to copy number changes with *in vitro* culture.

### *In Vitro* Determination of $IC_{50}$ Levels for Sal A-Selected Clones

$IC_{50}$ values were determined by testing parasites against two-fold serial dilutions of antimalarial compounds (Ekland et al., 2011). Compounds were tested in duplicate in 96-well plates, with 200 μL final volumes per well. Parasites were seeded at 0.2% parasitemia and 1% hematocrit. Serial dilutions and were performed on a Freedom Evo 100 liquid-handling instrument (Tecan). Parasites were continuously exposed to drugs for 72 h. After 72 h, cultures were cut 1:5 and continued in drug-free medium for an additional 48 h to

ensure complete parasite killing. After 120 h, parasites were stained with 1×SYBR Green and 100 nM MitoTracker Deep Red (ThermoFisher) and parasitemias were measured on an Intellicyt iQue3 flow cytometer sampling 10,0000–20,000 events per well. Data were analyzed using FlowJo and $IC_{50}$ values were derived using nonlinear regression analysis (GraphPad Prism).

### Chemical Synthesis of Salinipostin Alkyne

**15-hexadecyn-1-ol:** 1 g of NaH (42 mmol, 10 equiv.) was added to a dry round bottom flask under argon. 1,3-diaminopropane (15 mL, 180 mmol) was slowly added to the flask while stirring. The mixture was heated to 70°C and stirred for 1 h. After cooling to room temperature, 1 g of 7-hexadecyn-1-ol (4.2 mmol, dissolved in 4 mL 1,3-diaminopropane) was added to the flask and the reaction proceeded overnight at 55°C. The reaction was cooled to room temperature and ice cold $H_2O$ was added. The reaction mixture was acidified by the addition of 12% HCl. The organic layer was extracted 3× with ether, washed with saturated sodium bicarbonate and brine, and dried with $MgSO_4$. The organic layer was dried in vacuo and the resulting off-white powder was purified by silica column chromatography using EtOAc/hexanes step gradients (0%, 5%, 10%, 15%) to afford 15-hexadecyn-1-ol as a white solid in 57% yield. $^1$H NMR (400 MHz, Chloroform-d) δ 3.63 (t, *J* = 6.6 Hz, 2H), 2.17 (td, *J* = 7.1, 2.6 Hz, 2H), 1.93 (t, *J* = 2.6 Hz, 1H), 1.59 – 1.46 (m, 4H), 1.44 – 1.23 (m, 20H). $^{13}$C NMR (100 MHz, Chloroform-d) δ 84.96, 68.16, 63.20, 32.93, 29.80-29.70, 29.64, 29.57, 29.25, 28.90, 28.62, 25.87, 18.53.

**16-bromohexadec-1-yne:** To a solution of 15-hexadecyn-1-ol (150 mg, 0.63 mmol) in dichloromethane (3.7 mL) was added $CBr_4$ (313 mg, 0.95 mmol, 1.5 equiv.) and $PPh_3$ (248 mg, 0.95 mmol, 1.5 equiv.) and the reaction mixture was refluxed until the starting material was completely consumed by TLC analysis. The crude product was adsorbed onto celite, and purified using silica column chromatography (hexanes) to afford 16-bromohexadec-1-yne in 47% yield. $^1$H NMR (400 MHz, Chloroform-d) δ 3.39 (t, *J* = 6.9 Hz, 2H), 2.16 (td, *J* = 7.1, 2.7 Hz, 2H), 1.92 (t, *J* = 2.7 Hz, 1H), 1.83 (m, 2H), 1.57 (m, 2H), 1.44-1.34 (m, 4H), 1.31-1.25 (m, 16H). $^{13}$C NMR (100 MHz, Chloroform-d) δ 84.86, 68.15, 34.09, 32.97, 29.74-29.70, 29.66, 29.62, 29.56, 29.24, 28.90, 28.89, 28.63, 28.31, 18.52.

**Salinipostin alkyne (1):** A mixture of salinipostins A, B, and C (1.2 mg, ~2.7 μmol) and 16-bromohexadec-1-yne (18 mg, 60 μmol, 22 equiv.) were solubilized in 0.4 mL anhydrous dioxane. A catalytic amount of TBAI was added and the mixture was immersed in an oil bath preheated to 110°C and refluxed for 5 h. The reaction progress was monitored by LC/MS. After consumption of the starting material, the reaction mixture was dried and purified by semi-preparative HPLC (Agilent Zorbax 300SB-C18 column, 5 μm, 9.4 x 250 mm using a gradient of ACN:$H_2O$ + 0.1% TFA from 70-98% over 15 min to afford two diastereomers of salinipostin alkyne. Peak 1 (Salinipostin alkyne): $^1$H NMR (601 MHz, Chloroform-d) δ 4.43 (t, *J* = 9.0 Hz, 1H), 4.30 (dd, *J* = 18.9, 6.2 Hz, 1H), 4.23 – 4.12 (m, 2H), 4.04 (dd, *J* = 9.5, 5.8 Hz, 2H), 3.83 – 3.73 (m, 1H), 2.88 (ddt, *J* = 110.4, 14.2, 7.6 Hz, 2H), 2.18 (tdd, *J* = 7.1, 2.7, 1.0 Hz, 2H), 1.94 (td, *J* = 2.6, 1.0 Hz, 1H), 1.72 (p, *J* = 6.8 Hz, 2H), 1.64 – 1.47 (m, 4H), 1.43 – 1.34 (m, 6H), 1.26 (d, *J* = 7.7 Hz, 16H), 0.93 (td, *J* = 7.3, 1.0 Hz, 3H). $^{31}$P NMR- δ 12.24 (s).

Peak 2 (epi-Salinipostin alkyne): $^1$H NMR (601 MHz, Chloroform-d) δ 4.49 – 4.41 (m, 1H), 4.37 – 4.29 (m, 1H), 4.24 (dt, *J* = 8.0, 6.6 Hz, 2H), 4.14 (ddd, *J* = 25.7, 11.2, 3.6 Hz, 1H), 3.83 – 3.74 (m, 2H), 2.98 – 2.86 (m, 2H), 2.18 (tt, *J* = 5.4, 2.6 Hz, 2H), 1.94 (t, *J* = 2.6 Hz, 1H), 1.74 (p, *J* = 6.7 Hz, 2H), 1.53 (s, 4H), 1.40 (dt, *J* = 15.1, 7.4 Hz, 7H), 1.27 (d, *J* = 7.3 Hz, 15H), 0.96 – 0.90 (m, 3H). 31P NMR- δ 8.88 (s).

## QUANTIFICATION AND STATISTICAL ANALYSIS

All biochemical curves and statistical analyses were produced using Prism 6 (GraphPad Software). See individual sections above for details on the statistics used for analysis.

## DATA AND CODE AVAILABILITY

The mass spectrometry proteomics data have been deposited to the ProteomeXchange Consortium via the PRIDE (Perez-Riverol et al., 2019) partner repository with the dataset identifier PXD016835.